Vertical Land Motion from present-day deglaciation in the wider Arctic

Carsten Ludwigsen[1,1], Shfaqat Abbas Khan[2,2], Ole Baltazar Andersen[3,3], and Ben Marzeion[4,4]

[1]Technical Univeresity of Denmark
[2]DTU Space
[3]DTU Space, National Space Institute
[4]University of Bremen

November 30, 2022

Abstract

Vertical land motion (VLM) of Earth's surface can aggravate or mitigate ongoing relative sea level change. The near-linear process of Glacial Isostatic Adjustment (GIA) is normally assumed to govern regional VLM. However, present-day deglaciation of primarily the Greenland Ice Sheet causes a significant non-linear elastic uplift of >1 mm yr -1 in most of the wider Arctic. The elastic VLM exceeds GIA at 14 of 42 Arctic GNSS-sites, including sites in non-glaciated areas in the North Sea region and along the east coast of North America. The combined elastic VLM + GIA model is consistent with measured VLM at three-fourth of the GNSS-sites (R=0.74), which outperforms a GIA-only model (R=0.60). Deviations from GNSS-measured VLM, are interpreted as estimates of local circumstances causing VLM. Future accelerated ice loss on Greenland, will increase the significance of elastic uplift for North America and Northern Europe and become important for coastal sea level projections.

Vertical Land Motion from Present-Day Deglaciation in the Wider Arctic

Carsten Ankjær Ludwigsen[1], Shfaqat Abbas Khan[1], Ole Baltazar Andersen[1] and Ben Marzeion[2]

[1]DTU Space, Technical University of Denmark
[2]Institute of Geography and MARUM – Center for Marine Environmental Sciences, University of Bremen, Germany

Key Points:

- Elastic VLM from present-day ice loss in the Arctic causes significant uplift of coastlines in North America and Northern Europe.
- A combined VLM-model that includes GIA and elastic VLM, yields good agreement with GNSS-stations in the wider Arctic.
- Residuals between GNSS and modeled VLM provides an approximation of extraordinary VLM caused by local circumstances.

Corresponding author: Carsten Ankjær Ludwigsen, caanlu@space.dtu.dk

Abstract

Vertical land motion (VLM) from past and ongoing glacial changes can amplify or mitigate ongoing relative sea level change. We present a high resolution VLM-model for the wider Arctic, that includes both present-day ice loading (PDIL) and glacial isostatic adjustment (GIA). The study shows that the non-linear elastic uplift from PDIL is significant (0.5-1 mm y^{-1}) in most of the wider Arctic and exceeds GIA at 15 of 54 Arctic GNSS-sites, including sites in non-glaciated areas of the North Sea region and the east coast of North America. Thereby the sea level change from PDIL (1.85 mm y^{-1}) is significantly mitigated from VLM caused by PDIL. The combined VLM-model was consistent with measured VLM at 85% of the GNSS-sites (R=0.77) and outperformed a GIA-only model (R=0.64). Deviations from GNSS-measured VLM can be attributed to local circumstances causing VLM.

Plain Language Summary

From 2003 to 2015, the Northern Hemisphere lost more than 6,000 gigatons of land ice, which added nearly 18 mm to the global mean sea level rise. Loss of land-based ice results in the vertical deformation of the Earth's surface. Ongoing rebounding or subsidence caused by the end of the last ice age is often assumed to govern vertical deformation. However, present-day ice loss from Greenland and Arctic glaciers also cause an immediate vertical deformation. By using an vertical deformation model, that includes both components, we can explain GPS-measured deformation occurring in the Arctic. Our results show that the present-day Arctic ice loss contribution to vertical deformation is approximately 0.5 to 1 mm y^{-1} in the wider northern region. This exceeds deformation caused by the disappearance of the last ice ages at many coastal regions, including the North Sea region and the North American Atlantic coast. The Arctic present-day ice loss included in the VLM-model equals a global sea level rise of 1.5 mm y^{-1}, which means that 30-80% of the sea level rise caused by Arctic ice loss is mitigated by surface uplift caused by the same ice loss.

1 Introduction

The Arctic region is warming faster than any other region on Earth (Post et al., 2019). Deglaciation of Arctic land-based ice accounts for 70% of all barystatic sea level change (Abram et al., 2019) and has increased the sea level rise by 0.035 mm y^{-2} over the last three decades (Nerem et al., 2018). From 2003 to 2015 the Greenland Ice Sheet and adjoining glaciers produced 1 cm of sea level rise, while the contribution of other Arctic glaciers was 0.8 cm (Zemp et al., 2019).

Change in ice loading not only contributes to sea level change, but also alters Earth's solid surface, which commonly is called Vertical Land Motion (VLM). Accurate quantification of VLM and its causes is key for understanding relative sea level (RSL) (Watson et al., 2015; Wöppelmann & Marcos, 2016), which is the sea level change measured by tide gauges (TG).

VLM can be modeled for a given ice loading by employing the sea level equation of Farrell and Clark (1976) or in its elastic adaptation by Clark and Lingle (1977). viscoelastic relaxation of Earth's surface caused by past ice loading changes, also known as Glacial Isostatic Adjustment (GIA), has historically been the most important component of VLM (Farrell & Clark, 1976; Tushingham & Peltier, 1991; Milne & Mitrovica, 1998; Peltier et al., 2015) and is often assumed to be the key contributor to VLM in sea level studies from tide gauges (Church & White, 2011; Jevrejeva et al., 2014). This assumption is in particular inadequate in the Arctic region (Henry et al., 2012), where the change in present-day ice loading (PDIL) is extensive and the corresponding VLM equals GIA in order of magnitude.

Here we quantified the VLM resulting from changes in PDIL from 2003-2015 in the wider Arctic (the region above 50 deg latitude). After considering GIA, ocean loading, rotational feedback (RF) and non-secular geocenter motion, the total VLM uplift is predicted and compared to GNSS-measured VLM at 54 locations.

In recent years, data products from the Gravity Recovery And Climate Experiment (GRACE) satellite mission have been used to estimate PDIL and the corresponding VLM (Adhikari et al., 2016; Riva et al., 2017; Frederikse et al., 2019). While this is a reasonable estimate for regional and global VLM-patterns, the native resolution of GRACE is around 300-km half width at the equator (Tapley et al., 2004) which is insufficient for estimating VLM close to glaciers and ice sheets.

Here we combined a high-resolution (2x2 km) ice mass balance data in the Arctic to compute VLM from PDIL (VLM_{PDIL}), with a resolution that is suitable in both the near- and far-field in the Arctic region.

2 Data and Method

The solid-earth response of PDIL is assumed to be purely elastic and the viscoelastic response is considered to be negligible. This includes the ongoing solid-earth response from modern changes in ice loading prior to 2003, which is not considered in the applied GIA-models. In particular, the deglaciation after the Little Ice Age (LIA) that ended in the 19th century can create a GIA-like viscoelastic response that is not captured by GIA-models (Simon et al., 2018).

Contrary to studies using GRACE-measurements for ice loading, we used mass balance data from glaciers (Marzeion et al., 2012; Pfeffer et al., 2014; Zemp et al., 2019) that were transformed into an ice-elevation model (details in Supporting Information S1) with a 2x2 km spatial resolution by applying a mass balance distribution function and assuming a uniform density of 917 kg m^{-3}. Glaciers were combined with elevation changes from Greenland (updated version of the data from S. A. Khan et al. (2013), see section 2.1).

Separately, Antarctic yearly mass equivalent surface elevation changes for 2003-2015 from Schröder et al. (2019) were used to estimate the present-day Antarctic contribution to VLM in the Arctic.

The elastic VLM (VLM$_{PDIL}$) was computed with REAR (Regional Elastic Rebound calculator) (Melini et al., 2014, 2015). REAR calculates the elastic response to a disc load (Farrell, 1972) and assumes a solid, non-rotating and isotropic earth. Load Deformation Constants (LDC's) used for solving the Green's Functions were obtained from the REF6371 model by Kustowski et al. (2007) which is similar to the PREM-model (Dziewonski & Anderson, 1981), however the REF6371 model includes more realistic seismic properties of the crust (Kustowski et al., 2007). The LDC's from REAR are by default defined with respect to Earth's center of mass (CM-frame), which is consistent with the GIA-model of Caron et al. (2018). The ICE6G_D-model of Peltier et al. (2018) is referenced to the center of solid-earth (CE). The surface loading change included in GIA is however prehistoric and current viscoelastic mass transport induces a negligible CM-CE motion (King et al., 2012; Argus et al., 2014).

Rotational feedback (Milne & Mitrovica, 1998) was added to the elastic VLM-model by using equation 1 and 2 from King and Watson (2014). Position changes of the pole (x_p,y_p) for ITRF2008 are available from IERS (Bizouard & Gambis, 2009). Since REAR is not solving the sea level equation (Farrell & Clark, 1976; Milne et al., 1999), it does not account for the effect of extra water mass added to the oceans because of PDIL, which results in a measurable deformation (van Dam et al., 2012; Santamaría-Gómez & Mémin, 2015). Non-tidal ocean loading (NOL) is predicted by estimating the elastic deformation of ocean bottom pressure (OBP, shown in Figure S2.2 in Supporting Information) grids from the latest version of Estimating the Circulation and Climate of the Ocean (ECCO) project (version 4, release 4) (Fukumori et al., 2019; Forget et al., 2015).

GNSS data are referenced to ITRF2008 (Altamimi et al., 2011), which has secular trends in CM, while non-secular trends of ITRF are in center of figure (CF) (Dong et al., 2003). Therefore, when studying ongoing mass changes, we need to make a ITRF to CM translation by considering non-linear geocenter motion (GCM). GCM is obtained from first-order Stokes coefficients from 2002-2019 provided by Sun et al. (2016) available from `https://grace.jpl.nasa.gov/data/get-data/geocenter/`, which are detrended in order to make the ITRF to CM translation. An VLM-model (eq. 2) is created that is comparable to adjusted GNSS-measured VLM (eq. 3):

$$
\begin{aligned}
\mathrm{VLM}_{ela}^{CM} &= \mathrm{VLM}_{PDIL}^{CM} + \mathrm{VLM}_{NOL}^{CM} + \mathrm{VLM}_{rot} && (1)\\
\mathrm{VLM}_{model}^{CM} &= \mathrm{VLM}_{GIA}^{CM} + \mathrm{VLM}_{ela}^{CM} && (2)\\
\mathrm{VLM}_{GNSS}^{CM} &= \mathrm{VLM}_{GNSS}^{ITRF} - \mathrm{GCM}^{ITRF-CM} && (3)
\end{aligned}
$$

Where VLM_{ela}^{CM} is the elastic VLM-model, VLM_{GIA}^{CM} represents VLM caused by GIA, VLM_{rot} indicates the deformation caused by rotational feedback and VLM_{NOL} is the contribution from NOL. VLM_{GNSS}^{CM} is GNSS-measured VLM after non-secular geocenter motion is removed. Average VLM-rates from 2003-2015 are shown in Figure 1, while $\mathrm{VLM}_{model}^{CM}$ is evaluated against VLM_{GNSS}^{CM} in section 3. The contribution of Antarctic ice loading (including Southern Hemisphere glaciers) is shown together with the contribution of VLM_{NOL}^{CM} and VLM_{rot} in Figure S2.1 in Supporting Information.

Caron2018 (Caron et al., 2018) is the default GIA-model throughout this study. Caron2018 used 128000 forward models of different 1D Earth rheologies and ice elevation histories to create a statistical distribution of the GIA signal representative of long term GNSS observations and relative sea level records from paleo RSL indicators. In some parts of the analysis, we include the ICE-6G_D GIA model of Peltier et al. (2018), since large discrepancies between the $\mathrm{VLM}_{model}^{CM}$ and VLM_{GNSS}^{CM} can be explained by the choice of GIA-model. Recent study using an ensemble of simulations with 3D-earth rheologies (Li et al., 2020), seems to favor the results GIA-rates of Peltier et al. (2018).

Though we limited this study to the wider Arctic area, both the elastic VLM-components and GIA have a global impact. However, if we neglect the VLM caused by Antarctica, the VLM-signal from PDIL is relatively small ($< \pm 0.2$ mm y^{-1}) outside the region of this study. The estimated uncertainty of the VLM^{CM}_{model} originates from the standard uncertainty of the ice model combined with a 10% uncertainty that represents the uncertainity from the REF6371 earth model (Wang et al., 2012).

While the ice model of Greenland is well constrained, mass balance errors of individual glaciers from the glacial model can be large (several times the glacial signal). We therefore divide the glacial model into 25x25 km tiles, which reduces the uncertainty significantly, but might also introduce unrealistic low uncertainty in areas with large glacial signals or where glaciers are poorly constrained. Glaciers are, however, still the largest source of regional uncertainty (see Supporting Information Figure S3.1.). The Caron2018 GIA-model has standard uncertainty estimates included in the product, while there is no uncertainty estimate associated with the ICE6G-model. Uncertainties of geocenter motion from Sun et al. (2016) contributes to the GNSS-uncertainty estimate. The spatial distribution of the uncertainty estimates are shown in Supporting Information Figure S3.1.

2.1 Ice Loading

The main component of VLM_{PDIL} is the ice loading model and consist of a combined water equivalent elevation model from Greenland and mass balance estimates from glaciers. Rate of elevation change is shown in Supporting Information Figure S1.1. While only Northern Hemisphere ice history is created with high resolution, changes of Antarctic and Southern Hemisphere ice loading is computed on a 0.5x0.5° grid and included in the computation of VLM^{CM}_{PDIL}. The low resolution does not have any impact on VLM in the Arctic. The total mass loss of the Southern Hemisphere is 140 Gt y^{-1}, equivalent of to 0.38 mm y^{-1} barystatic sea level rise.

2.1.1 Glaciers

A total of 62,000 individual glaciers from the Randolph Glacier Inventory (RGI 6.0) (Pfeffer et al., 2014; RGI Consortium, 2017) located in North America, Russia, Scandinavia (incl. Svalbard) and Iceland have been included in this study. Mass loss from included glaciers accounts for 95 % of the registered glacial mass loss of the Northern Hemisphere and constitutes 80% of the global glacial mass loss (Zemp et al., 2019).

Mass change estimates for each glacier were estimated using an updated version of a model reported in Marzeion et al. (2012). Direct mass balance observations (Zemp et al., 2019) were used to calibrate and validate the glacier model. The glacier model translates information about atmospheric conditions into glacier mass change, while considering various feedback mechanisms that occur between glacier mass balance and glacier geometry. Glacial mass balance was combined with a distribution function to calculate glacier-wide surface elevation change. This ensured that the lower parts of glaciers are thinning, while upper parts experience small elevation gains. This 'slope steepening' of glaciers is characteristic of glaciers of many regions (Nuth et al., 2010; Foresta et al., 2016; Ciracì et al., 2018) and is assumed to apply to all glaciers included in this study (see Supporting Information S1 for an enhanced description of glacial elevation change).

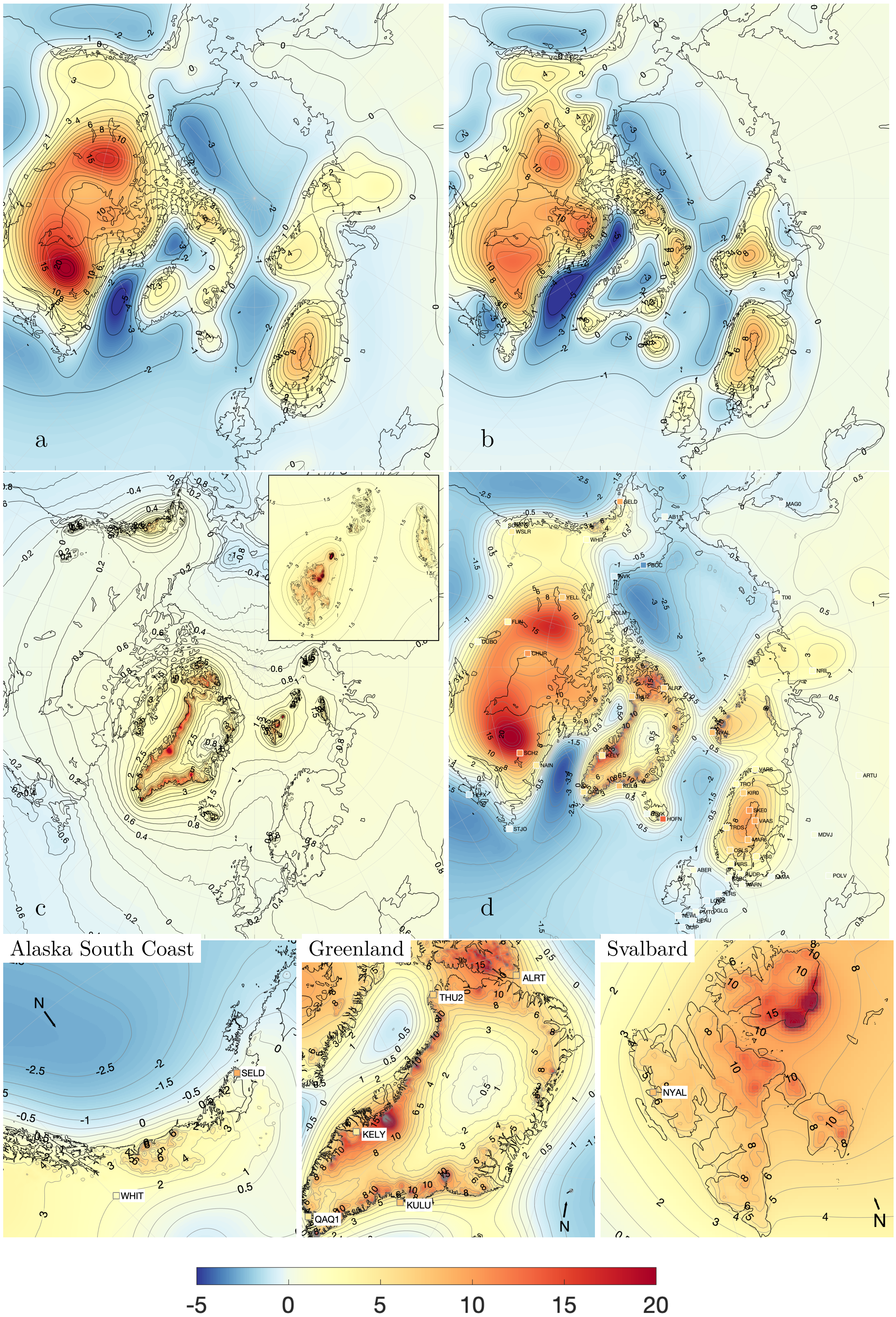

Figure 1. Average VLM-rates (mm y^{-1}) for 2003-2015 using the GIA-model of Caron2018(Caron et al., 2018) (a) and ICE6G_D (Peltier et al., 2018) (b). Modeled elastic rebound from contemporary land ice loss (including ocean loading and corrected for rotational feedback) (VLM_{ela}^{CM}) with enlargement of Svalbard is displayed in (c). The total VLM-model, VLM_{model}^{CM}, (a + c), with the square color representing average GNSS-determined VLM-rates (d). Enlargements of the south coast of Alaska, Greenland and Svalbard of (d) is shown in the bottom three panels. Spatial distribution of uncertainity estimates of (a),(c) and (d) are shown in Supporting Information Figure S3.1.

2.1.2 Greenland

Glacial ice history was combined with elevation change of the Greenland Ice Sheet and adjoining glaciers. We estimated the rate of ice volume change from 2003-2015 by using altimeter surveys from NASA's ATM flights (Krabill, 2011) that took place between 2003 and 2015 supplemented with high-resolution Ice, Cloud and land Elevation Satellite (ICESat) data (Zwally et al., 2011) from 2003-2009 and CryoSat-2 data from 2011-2015 (Helm et al., 2014). Our procedure for deriving ice surface elevation changes has previously been described in detail by S. A. Khan et al. (2013) and is similar to the method used by, e.g. Ewert et al. (2012); Smith et al. (2009) and Kjeldsen et al. (2013). We used the observed ice elevation change rates to interpolate (using collocation) ice elevation changes onto the 2x2 km spatial grid.

2.2 GNSS data

Timeseries of vertical deformation and uncertainty estimates of 54 GNSS-sites from the sixth release of the consortium led by University of La Rochelle (ULR-6) (Santamaría-Gómez et al., 2017) were used. A detailed map and timeseries of all GNSS-sites are shown in Supporting Information Figure S4.1 and Figure S5.1. ULR-6 includes 125 GNSS-sites located within the area of interest, but only GNSS-sites with data for at least 120 of 156 months from 2003 to 2015 known not to be impacted by human activities were selected. One GNSS site was selected based on lowest observed standard deviation of timeseries when multiple GNSS sites were located within 100 km of each other. Nome (AT11), Esbjerg City (ESBC) and Magadan (MAG0) were exempted from the temporal selection criteria, because of their location which has a special interest for interpretation.

Annual averages and combined uncertainties were calculated for each GNSS-site from the vertical component and standard uncertainty included in URL-6a. Hereafter, the linear trend was calculated for the years available between 2003 and 2015.

3 Evaluating the VLM model

From Figure 1 it is seen that the VLM-model is dominated by the pattern of the GIA-model, with rates above 20 mm y^{-1} east of the Hudson Bay and another local maximum of over 15 mm y^{-1} in north-west Canada. The elastic rebound is evident in most of the Arctic, particular in Greenland with large areas exceeding 10 mm y^{-1}, with maximum value at Jakobshavn Isbræ (69.1N, 49.5W) with an average modeled uplift of 40 mm y^{-1}. Large areas around Svalbard and Alaska have modeled elastic VLM-rates of more than 8 mm y^{-1}. The uncertainty is significantly larger in glaciated regions than in the far field (see Figure 3.1 in Supporting Information).

Most depression zones are found over the ocean, with the Beaufort Sea and Labrador Sea subsiding with 2 mm y^{-1} and the Norwegian Sea with 1.5 mm y^{-1}. Subsiding coastal areas are found in North America, where Nova Scotia and most of the US east- and west coast subsides with more than 1 mm y^{-1}, while smaller subsidence (0.0 - 0.5 mm y^{-1}) is found in Northern Europe along the North Sea and Atlantic coastlines. From Figure 1 we see that most subsiding areas are caused by GIA.

Figure 2 shows that $\mathrm{VLM}^{CM}_{model}$ predicts VLM within the range of VLM^{CM}_{GNSS} at 46 of 54 GNSS locations considered. The mean absolute error (MAE) for the 54 GNSS-sites was 1.45 mm y^{-1} (1.33 mm y^{-1} for ICE6G_D), which was 0.53 mm y^{-1} better than MAE from only VLM_{GIA}. For less than half (27) of the 54 GNSS-sites considered was the VLM-model with Caron2018 outperforming the ICE6G_D GIA model.

Barystatic sea level change for VLM_{PDIL} was 1.5 mm y^{-1} (ice loss-mediated global average sea level change (excl. Antarctica)). As shown in Figure 2, elastic VLM values

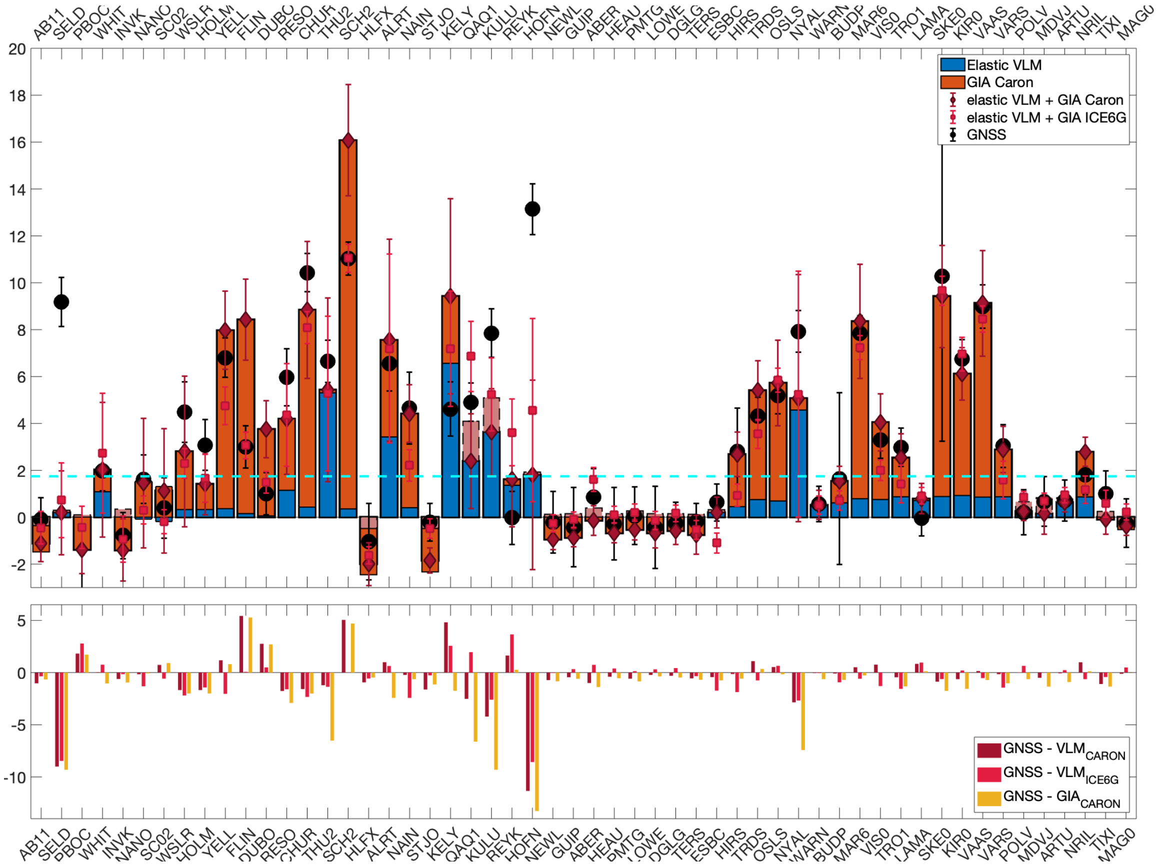

Figure 2. Average VLM change (mm y^{-1}) from 2003-2015 determined using the elastic VLM model (blue) and GIA (red) at the 54 GNSS-sites from Figure 1 and Supporting Information Figure S4.1 are shown (top). Sites are listed from most west (left) to most east (right). The dotted-cyan line indicates the average barystatic sea level rise ($\sim$ 1.85 mm y^{-1}) from the ice loss used in this study. The total modeled VLM uncertainty are indicated with red error bars and the GNSS-measured VLM is shown with black errorbars. Light red indicates locations in which GIA is negative and overlaps the positive elastic VLM. Residuals between GNSS-measured VLM (VLM$^{CM}_{GNSS}$) and the VLM-model (VLM$^{CM}_{model}$) (blue) and GIA (red) are shown (bottom). The average of the absolute residuals (equivalent to mean absolute error) are 1.45 mm y^{-1} and 1.98 mm y^{-1} respectively. All values used in this figure are included within Table S4.1 in Supporting Information.

between 0.5-1 mm y^{-1} were observed at many far field GNSS-sites in this study and partly mitigated the barystatic sea level change.

The effect of non-cryospheric mass change is not included in VLM$^{CM}_{model}$. In particular terrestial water storage (TWS) causes a small uplift over large parts of North America (0.4 - 0.8 mm y^{-1}) and North-Central Siberia (0.2 - 0.4 mm y^{-1}), while TWS is causing a subsidence in most of Scandinavia of 0.2 - 0.4 mm y^{-1} (Frederikse et al., 2019).

Glaciated regions show particularly large residuals between the predicted VLM and VLM measured by GNSS (Figure 3), but also exhibit the largest associated uncertainties of GNSS estimates. Predicted VLM at 26 of 54 GNSS-sites are within a range of 0.75 mm y^{-1} to GNSS (the three center bins in the right panel of Figure 3). The VLM-model has a tendency to underestimate the GNSS-measured VLM, which is evident in North

America and Europe. From figure 2, we see that a different choice of GIA-model would yield enhance the accuracy of the VLM-model in these regions. The most significant discrepancies between measured and predicted VLM is explained in the following for every region.

3.1 North America

Alaska is located in the transition zone between GIA-uplift and GIA-subsidence, which is also reflected in the GNSS-rates. Nome (AB11), Prudhoe Bay (PBOC) and Inuvik (INVK) all experience an GIA-subsidence that is larger than the elastic uplift. While Nome and INVK are well matched with VLM^{CM}_{GNSS}, PBUC has the largest measured subsidence (3.2 ± 1.6 mm y^{-1}), while $\mathrm{VLM}^{CM}_{model}$ only shows a subsidence of 1.4 ± 1.4 mm y^{-1}. An extraordinary subsidence is likely caused by oil extraction in the Prudhoe Bay area.

The Alaska south coast accounts for more than 25% of the total glacial melt and is naturally dominated by elastic uplift while the uplift from GIA is below 1 mm yr^{-1}. Seldovia (SELD) shows an observed average rate of 9.2 ± 1.0 mm yr^{-1}, while VLM^{CM}_{ela} is only 0.3 ± 1.6 mm yr^{-1} and GIA-rate -0.1 ± 0.8 mm yr^{-1}. Seldovia is located on the Kenai Peninsula close to the Kenai Fjords, which experienced an accelerated glacial ice loss in the 20th century (VanLooy et al., 2006). This is, however, not enough to explain the increased measured uplift. GIA-estimates vary in the region (Larsen et al., 2005; Hu & Freymueller, 2019), but is not more than around 1-2 mm yr^{-1}. The residual seems explained by a postseismic signal following the Prince Willam Sound Earthquake in 1964 (Cohen & Freymueller, 2001; Huang et al., 2020) which is still causing a local uplift on this side of the peninsula. The residuals estimates this effect to be 9.0 mm yr^{-1} from 2003-2015, which is slightly less than the value found by Cohen and Freymueller (2001) of 9.3 mm yr^{-1} from 1994-2001. This rebound is expected to decay further over time, but will still be relevant for decades to come (Cohen & Freymueller, 2001; Huang et al., 2020).

Discrepancies between GNSS and modeled VLM in central North America, are likely due to uncertain GIA-estimates. A significantly better alignment between $\mathrm{VLM}^{CM}_{model}$ and GNSS is reached if Caron2018 is replaced by ICE-6G. The GIA-overestimate of Caron2018 in North America has been demonstrated by other studies (Schumacher et al., 2018; Frederikse et al., 2019) and is likely caused by large differences between estimated viscosity properties of paleo-RSL indicators and GNSS in North America (Caron et al., 2018). TWS-change causes a small uplift below 1 mm y^{-1} over large parts of North America (Frederikse et al., 2019), which enhances the difference between $\mathrm{VLM}^{CM}_{model}$ and VLM^{CM}_{GNSS}.

3.2 Greenland

Four GNSS-sites on Greenland and Alert (ALRT) on Baffin Island measure a significant elastic uplift. While Pittuffik/Thule (THU2) and ALRT agree with $\mathrm{VLM}^{CM}_{model}$, Kangerlussuaq (KELY) is overestimated quite a bit and $\mathrm{VLM}^{CM}_{model}$ at Kulusuk (KULU) and Qaqortoq (QAQ1) is below VLM^{CM}_{GNSS}. GIA on Greenland is poorly constrained in Caron2018, which can exaggerate VLM-estimates from GIA. A low-viscosity zone stretching from Iceland beneath Southeast Greenland (S. A. Khan et al., 2016) enables a significant viscoelastic rebound caused by ice loss since LIA (S. Khan et al., 2014).

3.3 Iceland

The two GNSS-sites on Iceland show very different uplift rates of 0.0 ± 1.1 mm yr^{-1} in Reykjavik (REYK) and 13.1 ± 1.1 mm yr^{-1} at Hoefn (HOFN) at the southern edge of the largest ice cap on Iceland, Vatnajökull. $\mathrm{VLM}^{CM}_{model}$ overestimates the rebound in Reykjavik while it largely underestimates it at Hoefn. Similar to south east Greenland a soft viscoelastic mantle layer (Fleming et al., 2007) creates a present-day viscoelas-

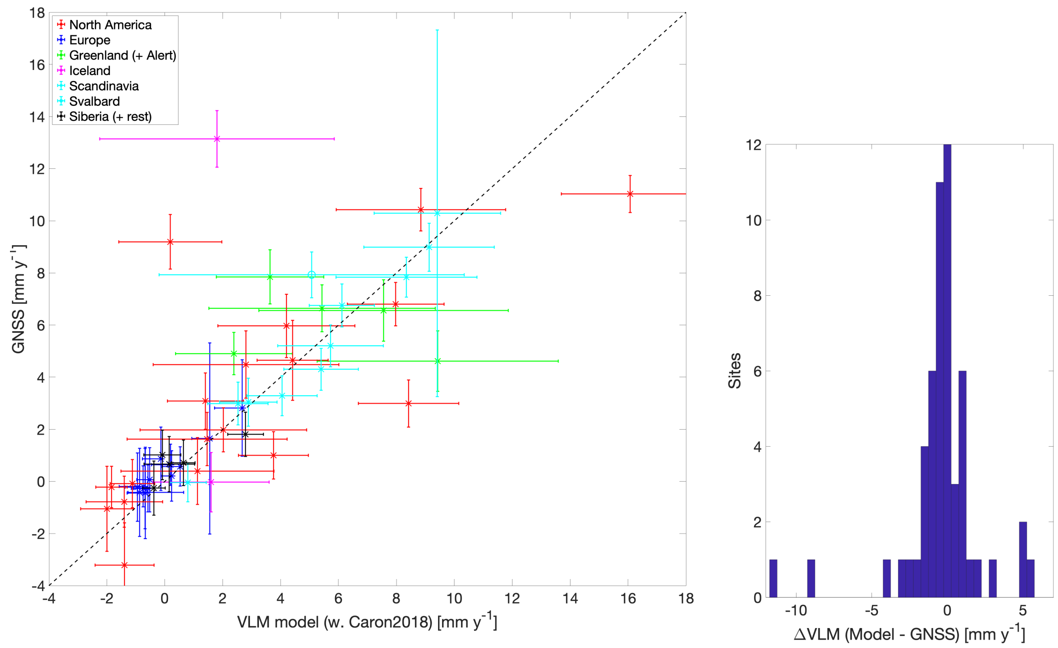

Figure 3. VLM^{CM}_{GNSS} versus $\mathrm{VLM}^{CM}_{model}$ including associated uncertainties for all GNSS-sites. If the cross is above the dashed line the $\mathrm{VLM}^{CM}_{model}$ underestimate compared to VLM^{CM}_{GNSS}. A histogram of the difference between $\mathrm{VLM}^{CM}_{model}$ and VLM^{CM}_{GNSS} (in intervals of 0.5 mm y^{-1}) is shown in the right panel.

tic signal that is much larger than the ones predicted by the GIA-model. A thin crust, also means that the uplift decreases faster with distance to the glacier (Fleming et al., 2007; Sørensen et al., 2017), which could explain why Reykjavik shows little vertical deformation despite being less than 100 km from glaciers.

3.4 Svalbard

The majority of land in Svalbard is covered with ice, and VLM is highly affected by ongoing ice-mass changes. At Ny Ålesund (NYAL), located on the west coast, $\mathrm{VLM}^{CM}_{model}$ is dominated by VLM^{CM}_{ela} of 4.6 ± 5.3 mm yr^{-1} and VLM_{GIA} of 0.5± 0.4 mm yr^{-1}. In total this is 2.6 mm yr^{-1} short of observed VLM^{CM}_{GNSS}. While ICE6G and Caron2018 agree within ± 0.2 mm yr^{-1}, more focused, but older studies predict a slightly higher GIA contribution of around 1.5 mm yr^{-1} (Sato et al., 2006; Kierulf et al., 2009). Also on Svalbard, significant post-LIA deglaciation (Grove, 2001) is likely contributing to an ongoing uplift (Mémin et al., 2014; Rajner, 2018). The effect is still uncertain (Rajner, 2018) and Mémin et al. (2014) estimated the post-LIA rebound to be 2-5 mm yr^{-1} in the beginning of 21st century, which explains the residual of 2.9 mm yr^{-1}.

3.5 Northern Europe and Scandinavia

GIA is dominating the vertical deformation in Scandinavia (Figure 1). Even though small glaciers exist in Norway, the elastic effect is very local and has almost negligible effect on the GNSS-sites in this study. However, VLM^{CM}_{ela} is still significant, and improves the correlation with observed VLM^{CM}_{GNSS} compared to a GIA-only model. This becomes more prominent for GNSS-sites in areas, where GIA is less dominant. Esbjerg (ESBC) on the west coast of Denmark is close to the zero-line of Caron2018 (-0.1 mm yr^{-1}), but is still measuring an uplift of about 0.6 mm yr^{-1}, which is partly explained by an elastic uplift of 0.3 mm yr^{-1}.

In Northern Europe, Caron2018 models a subsidence, which is mitigated by an elastic uplift caused by present day ice melt. Generally, VLM$^{CM}_{model}$ is consistent with VLM$^{CM}_{GNSS}$ in the North Sea and the Baltic region, while an VLM-model using ICE6G is at odds at several locations.

3.6 Siberia

Only a few available GNSS measurements exist in eastern Europe and Siberia. Caron2018 is also challenged by limited resources of paleo sea-level records, which makes the GIA-model more dependent on the existing GNSS-records. It is commonly anticipated that Siberia had little or no ice during the last glacial cycle (Whitehouse et al., 2007), except north central Siberia and in the shallow waters in the Barents Sea between Svalbard and Novaya Zemlya (Root et al., 2015).

Also VLM$^{CM}_{ela}$ is generally smaller than around 1 mm yr^{-1}. While the VLM$^{CM}_{GNSS}$ is within the uncertainty-range of VLM$^{CM}_{model}$ for the Siberian GNSS-sites (Arti (ARTU), Norilsk (NRIL), Tixi (TIXI) and Magadan (MAG0)), a GIA-only model has a better fit to the GNSS measurements which is likely due to increased dependence on GNSS in Caron2018.

4 Discussion and Conclusion

VLM of the wider Arctic region occurs mainly as a result GIA and elastic VLM. Though this study is limited to the area surrounding the Arctic, VLM caused by deglaciation produces global effects (Riva et al., 2017; Kleinherenbrink et al., 2018; Frederikse et al., 2019). By combining deglaciation that occurred since the last glacial maximum (GIA) and present-day changes in land ice (elastic VLM), the VLM-model provides a realistic estimate of VLM in the Arctic. By evaluating 54 GNSS-sites using a combined VLM-model, we found that measured uplift of GNSS can be explained by either prehistoric or present-day changes in land ice volume. For 46 of the GNSS sites, residuals between GNSS-measured VLM values and the VLM-model were smaller than associated uncertainties.

The 2x2-km spatial resolution of the used ice-model was much higher than similar gravimetric satellite observations from GRACE (Adhikari et al., 2019). Increased spatial resolution improves VLM predictions accuracy in glaciated regions significantly, as local elastic deformation tends to dominate regional averages observed via GRACE (Frederikse et al., 2019). A VLM-model to GNSS comparison also indicated that the VLM-model was inadequate in some regions due to local causes of VLM that were not included in the VLM-model, such as subsurface properties, past seismic activity or 19–20th century ice-loss (Mémin et al., 2014; Rajner, 2018).

In non-glaciated areas, GNSS measurements generally agree well with the VLM-model. Contour lines shown in Figure 1, indicate that elastic uplift is centered around Greenland, except when close to other glaciated regions (e.g. Alaska and Svalbard), despite the fact that total Arctic glaciers mass loss is comparable with that of Greenland. Hence, the elastic uplift caused by ice melt in Greenland significantly affects the entire wider Arctic region, which includes coastlines of Northern Europe and the North American Atlantic.

Riva et al. (2017) showed that elastic uplift caused by ice loss in Greenland causes a subsidence in the Southern Hemisphere. Similar, it is assumed that Antarctic ice loss will cause a subsidence in the Northern Hemisphere. Antarctic ice loss averaged 105 Gt y^{-1} from 2003-2015 (Schröder et al., 2019), and resulted in an elastic subsidence of less than 0.1 mm y^{-1} in the Northern Hemisphere. Since ice loss has the potential to occur rapidly in the future (Hay et al., 2017; Edwards et al., 2019), VLM caused by Antarctic ice loss will be increasingly significant, and may be important for future coastal sea level projections in the Northern Hemisphere.

Acknowledgments

We wish to thank Lambert Caron, Matt King and one anonymous reviewer for their constructive and helpful comments, which greatly improved the manuscript. Thanks to Danielle Melini (Melini et al., 2014), for creating the REAR-code, which facilitated the creation of the VLM-model. We also greatly appreciate the work of L. Caron (Caron et al., 2018) on the Caron2018 GIA-model available from the NASA JPL website (https://vesl.jpl.nasa.gov/solid-earth/gia/) and R. Peltier on the ICE-6G_D model (Peltier et al., 2018). elastic VLM and both GIA-models is available in a Arctic 5x5 km grid at data.dtu.dk/articles/Arctic_Vertical_Land_Motion_5x5_km_/12554489. The project was partially funded by the EU-INTAROS project (Grant agreement no. 727890) and the ESA-Climate Change Initiative Sea level budget closure (Expro RFP/3-14679/16/I-NB).

References

Abram, N., Adler, C., Bindoff, N., Cheng, L., Cheong, S.-M., Cheung, W., … Zhai, P. (2019, 09). Summary for policymakers. in: IPCC special report on the ocean and cryosphere in a changing climate..

Adhikari, S., Ivins, E. R., Frederikse, T., Landerer, F. W., & Caron, L. (2019). Sea-level fingerprints emergent from grace mission data. *Earth System Science Data*, *11*(2), 629–646. Retrieved from https://www.earth-syst-sci-data.net/11/629/2019/ doi: 10.5194/essd-11-629-2019

Adhikari, S., Ivins, E. R., & Larour, E. (2016). Issm-sesaw v1.0: mesh-based computation of gravitationally consistent sea-level and geodetic signatures caused by cryosphere and climate driven mass change. *Geoscientific Model Development*, *9*(3), 1087–1109. Retrieved from https://www.geosci-model-dev.net/9/1087/2016/ doi: 10.5194/gmd-9-1087-2016

Altamimi, Z., Collilieux, X., & Métivier, L. (2011). Itrf2008: an improved solution of the international terrestrial reference frame. *Journal of Geodesy*, *85*(8), 457–473. Retrieved from https://doi.org/10.1007/s00190-011-0444-4 doi: 10.1007/s00190-011-0444-4

Argus, D., Peltier, W., Drummond, R., & Moore, A. (2014). The antarctica component of postglacial rebound model ice-6g_c (vm5a) based on gps positioning, exposure age dating of ice thicknesses, and relative sea level histories. *Geophysical Journal International*, *198*(1), 537-563. Retrieved from https://www.scopus.com/inward/record.uri?eid=2-s2.0-84905924704&doi=10.1093%2fgji%2fggu140&partnerID=40&md5=10f1208c9a63c67153b06b8bd607a133 (cited By 149) doi: 10.1093/gji/ggu140

Bizouard, C., & Gambis, D. (2009, 06). The combined solution c04 for earth orientation parameters consistent with international terrestrial reference frame 2005. In (Vol. 134, p. 265-270). doi: 10.1007/978-3-642-00860-3_41

Caron, L., Ivins, E. R., Larour, E., Adhikari, S., Nilsson, J., & Blewitt, G. (2018). Gia model statistics for grace hydrology, cryosphere, and ocean science. *Geophysical Research Letters*, *45*(5), 2203-2212. Retrieved from https://agupubs.onlinelibrary.wiley.com/doi/abs/10.1002/2017GL076644 doi: 10.1002/2017GL076644

Church, J., & White, N. (2011). Sea-level rise from the late 19th to the early 21st century. *Surveys in Geophysics*, *32*(4-5), 585-602. Retrieved from https://www.scopus.com/inward/record.uri?eid=2-s2.0-80053195533&doi=10.1007%2fs10712-011-9119-1&partnerID=40&md5=

a6a2b9bb53f622e9bf4b3266a27d54f0 (cited By 737) doi: 10.1007/s10712-011-9119-1

Ciracì, E., Velicogna, I., & Sutterley, T. C. (2018). Mass balance of novaya zemlya archipelago, russian high arctic, using time-variable gravity from grace and altimetry data from icesat and cryosat-2. *Remote Sensing*, *10*(11). Retrieved from https://www.mdpi.com/2072-4292/10/11/1817 doi: 10.3390/rs10111817

Clark, J. A., & Lingle, C. S. (1977). Future sea-level changes due to west antarctic ice sheet fluctuations. *Nature*, *269*(5625), 206–209. Retrieved from https://doi.org/10.1038/269206a0 doi: 10.1038/269206a0

Cohen, S. C., & Freymueller, J. T. (2001). Crustal uplift in the south central alaska subduction zone: New analysis and interpretation of tide gauge observations. *Journal of Geophysical Research: Solid Earth*, *106*(B6), 11259-11270. Retrieved from https://agupubs.onlinelibrary.wiley.com/doi/abs/10.1029/2000JB900419 doi: 10.1029/2000JB900419

Dong, D., Yunck, T., & Heflin, M. (2003). Origin of the international terrestrial reference frame. *Journal of Geophysical Research: Solid Earth*, *108*(B4). Retrieved from https://agupubs.onlinelibrary.wiley.com/doi/abs/10.1029/2002JB002035 doi: 10.1029/2002JB002035

Dziewonski, A. M., & Anderson, D. L. (1981). Preliminary reference earth model. *Physics of the Earth and Planetary Interiors*, *25*(4), 297 - 356. Retrieved from http://www.sciencedirect.com/science/article/pii/0031920181900467 doi: https://doi.org/10.1016/0031-9201(81)90046-7

Edwards, T., Brandon, M., Durand, G., Edwards, N., Golledge, N., Holden, P., … Wernecke, A. (2019, 02). Revisiting antarctic ice loss due to marine ice-cliff instability. *Nature*, *566*, 58-64. doi: 10.1038/s41586-019-0901-4

Ewert, H., Groh, A., & Dietrich, R. (2012, September). Volume and mass changes of the Greenland ice sheet inferred from ICESat and GRACE. *Journal of Geodynamics*, *59-60*, 111-123. doi: 10.1016/j.jog.2011.06.003

Farrell, W. E. (1972). Deformation of the earth by surface loads. *Reviews of Geophysics*, *10*(3), 761-797. Retrieved from https://agupubs.onlinelibrary.wiley.com/doi/abs/10.1029/RG010i003p00761 doi: 10.1029/RG010i003p00761

Farrell, W. E., & Clark, J. A. (1976). On postglacial sea level. *Geophysical Journal of the Royal Astronomical Society*, *46*(3), 647-667. Retrieved from https://onlinelibrary.wiley.com/doi/abs/10.1111/j.1365-246X.1976.tb01252.x doi: 10.1111/j.1365-246X.1976.tb01252.x

Fleming, K., Martinec, Z., & Wolf, D. (2007, 01). Glacial-isostatic adjustment and the viscosity structure underlying the vatnajökull ice cap, iceland. *Pure and Applied Geophysics*, *164*, 751-768. doi: 10.1007/s00024-007-0187-6

Foresta, L., Gourmelen, N., Pálsson, F., Nienow, P., Björnsson, H., & Shepherd, A. (2016). Surface elevation change and mass balance of icelandic ice caps derived from swath mode cryosat-2 altimetry. *Geophysical Research Letters*, *43*(23), 12,138-12,145. Retrieved from https://agupubs.onlinelibrary.wiley.com/doi/abs/10.1002/2016GL071485 doi: 10.1002/2016GL071485

Forget, G., Campin, J.-M., Heimbach, P., Hill, C. N., Ponte, R. M., & Wunsch, C. (2015). Ecco version 4: an integrated framework for non-linear inverse modeling and global ocean state estimation. *Geoscientific Model Development*, *8*(10), 3071–3104. Retrieved from https://gmd.copernicus.org/articles/8/3071/2015/ doi: 10.5194/gmd-8-3071-2015

Frederikse, T., Landerer, F. W., & Caron, L. (2019). The imprints of contemporary mass redistribution on local sea level and vertical land motion observations. *Solid Earth*, *10*(6), 1971–1987. Retrieved from https://www.solid-earth.net/10/1971/2019/ doi: 10.5194/se-10-1971-2019

Fukumori, I., Wang, O., Fenty, I., Forget, G., Heimbach, P., & Ponte, R. M. (2019).

Ecco version 4 release 4 dataset. https://ecco.jpl.nasa.gov/drive. (Accessed: 2020-06-25)

Grove, J. (2001, 01). The initiation of the "little ice age" in regions round the north atlantic. *Climatic Change*, *48*, 53-82. doi: 10.1023/A:1005662822136

Hay, C. C., Lau, H. C. P., Gomez, N., Austermann, J., Powell, E., Mitrovica, J. X., … Wiens, D. A. (2017). Sea level fingerprints in a region of complex earth structure: The case of wais. *Journal of Climate*, *30*(6), 1881-1892. Retrieved from https://doi.org/10.1175/JCLI-D-16-0388.1 doi: 10.1175/JCLI-D-16-0388.1

Helm, V., Humbert, A., & Miller, H. (2014). Elevation and elevation change of greenland and antarctica derived from cryosat-2. *The Cryosphere*, *8*(4), 1539–1559. Retrieved from https://www.the-cryosphere.net/8/1539/2014/ doi: 10.5194/tc-8-1539-2014

Henry, O., Prandi, P., Llovel, W., Cazenave, A., Jevrejeva, S., Stammer, D., … Koldunov, N. (2012). Tide gauge-based sea level variations since 1950 along the norwegian and russian coasts of the arctic ocean: Contribution of the steric and mass components. *Journal of Geophysical Research: Oceans*, *117*(C6). Retrieved from https://agupubs.onlinelibrary.wiley.com/doi/abs/10.1029/2011JC007706 doi: 10.1029/2011JC007706

Hu, Y., & Freymueller, J. T. (2019). Geodetic observations of time-variable glacial isostatic adjustment in southeast alaska and its implications for earth rheology. *Journal of Geophysical Research: Solid Earth*, *124*(9), 9870-9889. Retrieved from https://agupubs.onlinelibrary.wiley.com/doi/abs/10.1029/2018JB017028 doi: 10.1029/2018JB017028

Huang, K., Hu, Y., & Freymueller, J. T. (2020). Decadal viscoelastic postseismic deformation of the 1964 mw9.2 alaska earthquake. *Journal of Geophysical Research: Solid Earth*, e2020JB019649. Retrieved from https://agupubs.onlinelibrary.wiley.com/doi/abs/10.1029/2020JB019649 (e2020JB019649 2020JB019649) doi: 10.1029/2020JB019649

Jevrejeva, S., Moore, J., Grinsted, A., Matthews, A., & Spada, G. (2014). Trends and acceleration in global and regional sea levels since 1807. *Global and Planetary Change*, *113*, 11-22. Retrieved from https://www.scopus.com/inward/record.uri?eid=2-s2.0-84890953576&doi=10.1016%2fj.gloplacha.2013.12.004&partnerID=40&md5=67194675f8fc061f1bb025a9fb67361f (cited By 85) doi: 10.1016/j.gloplacha.2013.12.004

Khan, S., Kjeldsen, K., Kjær, K., Bevan, S., Luckman, A., Aschwanden, A., … Fitzner, A. (2014). Glacier dynamics at helheim and kangerdlugssuaq glaciers, southeast greenland, since the little ice age. *Cryosphere*, *8*, 1497–1507. (CC Attribution 3.0 License) doi: 10.5194/tc-8-1497-2014

Khan, S. A., Kjær, K. H., Korsgaard, N. J., Wahr, J., Joughin, I. R., Timm, L. H., … Babonis, G. (2013). Recurring dynamically induced thinning during 1985 to 2010 on upernavik isstrøm, west greenland. *Journal of Geophysical Research: Earth Surface*, *118*(1), 111-121. Retrieved from https://agupubs.onlinelibrary.wiley.com/doi/abs/10.1029/2012JF002481 doi: 10.1029/2012JF002481

Khan, S. A., Sasgen, I., Bevis, M., van Dam, T., Bamber, J. L., Wahr, J., … Munneke, P. K. (2016). Geodetic measurements reveal similarities between post–last glacial maximum and present-day mass loss from the greenland ice sheet. *Science Advances*, *2*(9). Retrieved from https://advances.sciencemag.org/content/2/9/e1600931 doi: 10.1126/sciadv.1600931

Kierulf, H. P., Plag, H.-P., & Kohler, J. (2009, 10). Surface deformation induced by present-day ice melting in Svalbard. *Geophysical Journal International*, *179*(1), 1-13. Retrieved from https://doi.org/10.1111/j.1365-246X.2009.04322.x doi: 10.1111/j.1365-246X.2009.04322.x

King, M. A., Keshin, M., Whitehouse, P. L., Thomas, I. D., Milne, G., & Riva,

R. E. M. (2012). Regional biases in absolute sea-level estimates from tide gauge data due to residual unmodeled vertical land movement. *Geophysical Research Letters*, *39*(14). Retrieved from https://agupubs.onlinelibrary.wiley.com/doi/abs/10.1029/2012GL052348 doi: 10.1029/2012GL052348

King, M. A., & Watson, C. S. (2014, 09). Geodetic vertical velocities affected by recent rapid changes in polar motion. *Geophysical Journal International*, *199*(2), 1161-1165. Retrieved from https://doi.org/10.1093/gji/ggu325 doi: 10.1093/gji/ggu325

Kjeldsen, K. K., Khan, S. A., Wahr, J., Korsgaard, N. J., Kjær, K. H., Bjørk, A. A., … van Angelen, J. H. (2013). Improved ice loss estimate of the northwestern greenland ice sheet. *Journal of Geophysical Research: Solid Earth*, *118*(2), 698-708. Retrieved from https://agupubs.onlinelibrary.wiley.com/doi/abs/10.1029/2012JB009684 doi: 10.1029/2012JB009684

Kleinherenbrink, M., Riva, R., & Frederikse, T. (2018). A comparison of methods to estimate vertical land motion trends from gnss and altimetry at tide gauge stations. *Ocean Science*, *14*(2), 187-204. Retrieved from https://www.scopus.com/inward/record.uri?eid=2-s2.0-85044121271&doi=10.5194%2fos-14-187-2018&partnerID=40&md5=dbe85241ab9f3400fe3f655c42918079 (cited By 6) doi: 10.5194/os-14-187-2018

Krabill, W. B. (2011). *Icebridge atm l2 icessn elevation, slope, and roughness, [1993-2012].* (Boulder, Colorado: NASA Distributed Active Archive Center at the National Snow and Ice Data Center) doi: 10.5067/ICESAT/GLAS/DATA225

Kustowski, B., Dziewoński, A. M., & Ekström, G. (2007, 10). Nonlinear Crustal Corrections for Normal-Mode Seismograms. *Bulletin of the Seismological Society of America*, *97*(5), 1756-1762. Retrieved from https://doi.org/10.1785/0120070041 doi: 10.1785/0120070041

Larsen, C. F., Motyka, R. J., Freymueller, J. T., Echelmeyer, K. A., & Ivins, E. R. (2005). Rapid viscoelastic uplift in southeast alaska caused by post-little ice age glacial retreat. *Earth and Planetary Science Letters*, *237*(3), 548 - 560. Retrieved from http://www.sciencedirect.com/science/article/pii/S0012821X05004152 doi: https://doi.org/10.1016/j.epsl.2005.06.032

Li, T., Wu, P., Wang, H., Steffen, H., Khan, N. S., Engelhart, S. E., … Horton, B. P. (2020). Uncertainties of glacial isostatic adjustment model predictions in north america associated with 3d structure. *Geophysical Research Letters*, *47*(10), e2020GL087944. Retrieved from https://agupubs.onlinelibrary.wiley.com/doi/abs/10.1029/2020GL087944 (e2020GL087944 2020GL087944) doi: 10.1029/2020GL087944

Marzeion, B., Jarosch, A. H., & Hofer, M. (2012). Past and future sea-level change from the surface mass balance of glaciers. *The Cryosphere*, *6*(6), 1295–1322. Retrieved from https://www.the-cryosphere.net/6/1295/2012/ doi: 10.5194/tc-6-1295-2012

Melini, D., Gegout, P., King, M., Marzeion, B., & Spada, G. (2015, 08). On the rebound: Modeling earth's ever-changing shape. *Eos Transactions American Geophysical Union*, *96*. doi: 10.1029/2015EO033387

Melini, D., Spada, G., Gegout, P., & King, M. (2014, 01). *Rear - a regional elastic rebound calculator. user manual for version 1.0.* Retrieved from http://hpc.rm.ingv.it/rear

Milne, G. A., & Mitrovica, J. X. (1998, 04). Postglacial sea-level change on a rotating Earth. *Geophysical Journal International*, *133*(1), 1-19. Retrieved from https://doi.org/10.1046/j.1365-246X.1998.1331455.x doi: 10.1046/j.1365-246X.1998.1331455.x

Milne, G. A., Mitrovica, J. X., & Davis, J. L. (1999, 11). Near-field hydro-isostasy: the implementation of a revised sea-level equation. *Geophysical Journal International*, *139*(2), 464-482. Retrieved from https://doi.org/10.1046/j.1365

-246x.1999.00971.x doi: 10.1046/j.1365-246x.1999.00971.x

Mémin, A., Spada, G., Boy, J.-P., Rogister, Y., & Hinderer, J. (2014, 05). Decadal geodetic variations in Ny-Ålesund (Svalbard): role of past and present ice-mass changes . *Geophysical Journal International*, *198*(1), 285-297. Retrieved from https://doi.org/10.1093/gji/ggu134 doi: 10.1093/gji/ggu134

Nerem, R. S., Beckley, B. D., Fasullo, J. T., Hamlington, B. D., Masters, D., & Mitchum, G. T. (2018). Climate-change–driven accelerated sea-level rise detected in the altimeter era. *Proceedings of the National Academy of Sciences*, *115*(9), 2022–2025. Retrieved from https://www.pnas.org/content/115/9/2022 doi: 10.1073/pnas.1717312115

Nuth, C., Moholdt, G., Kohler, J., Hagen, J. O., & Kääb, A. (2010). Svalbard glacier elevation changes and contribution to sea level rise. *Journal of Geophysical Research: Earth Surface*, *115*(F1). Retrieved from https://agupubs.onlinelibrary.wiley.com/doi/abs/10.1029/2008JF001223 doi: 10.1029/2008JF001223

Peltier, W., Argus, D., & Drummond, R. (2015). Space geodesy constrains ice age terminal deglaciation: The global ice-6g-c (vm5a) model. *Journal of Geophysical Research: Solid Earth*, *120*(1), 450-487. Retrieved from https://www.scopus.com/inward/record.uri?eid=2-s2.0-85027948080&doi=10.1002%2f2014JB011176&partnerID=40&md5=29a7ce38c5cf3872d2276981d2f6b34f (cited By 326) doi: 10.1002/2014JB011176

Peltier, W. R., Argus, D. F., & Drummond, R. (2018, February). Comment on "An Assessment of the ICE-6G_C (VM5a) Glacial Isostatic Adjustment Model" by Purcell et al. *Journal of Geophysical Research (Solid Earth)*, *123*(2), 2019-2028. doi: 10.1002/2016JB013844

Pfeffer, W. T., Arendt, A. A., Bliss, A., Bolch, T., Cogley, J. G., Gardner, A. S., … et al. (2014). The randolph glacier inventory: a globally complete inventory of glaciers. *Journal of Glaciology*, *60*(221), 537–552. doi: 10.3189/2014JoG13J176

Post, E., Alley, R. B., Christensen, T. R., Macias-Fauria, M., Forbes, B. C., Gooseff, M. N., … Wang, M. (2019). The polar regions in a 2c warmer world. *Science Advances*, *5*(12). Retrieved from https://advances.sciencemag.org/content/5/12/eaaw9883 doi: 10.1126/sciadv.aaw9883

Rajner, M. (2018). Detection of ice mass variation using gnss measurements at svalbard. *Journal of Geodynamics*, *121*, 20 - 25. Retrieved from http://www.sciencedirect.com/science/article/pii/S0264370718300450 doi: https://doi.org/10.1016/j.jog.2018.06.001

RGI Consortium. (2017). *Randolph Glacier Inventory – A Dataset of Global Glacier Outlines: Version 6.0: Technical Report.* (https://doi.org/10.7265/N5-RGI-60)

Riva, E., Frederikse, T., King, A., Marzeion, B., & Van Den Broeke, R. (2017). Brief communication: The global signature of post-1900 land ice wastage on vertical land motion. *Cryosphere*, *11*(3), 1327-1332. Retrieved from https://www.scopus.com/inward/record.uri?eid=2-s2.0-85020484420&doi=10.5194%2ftc-11-1327-2017&partnerID=40&md5=077251aec38900cef0ec0ecdd2b1eded (cited By 11) doi: 10.5194/tc-11-1327-2017

Root, B. C., Tarasov, L., & van der Wal, W. (2015). Grace gravity observations constrain weichselian ice thickness in the barents sea. *Geophysical Research Letters*, *42*(9), 3313-3320. Retrieved from https://agupubs.onlinelibrary.wiley.com/doi/abs/10.1002/2015GL063769 doi: 10.1002/2015GL063769

Santamaría-Gómez, A., Gravelle, M., Dangendorf, S., Marcos, M., Spada, G., & Wöppelmann, G. (2017). Uncertainty of the 20th century sea-level rise due to vertical land motion errors. *Earth and Planetary Science Letters*, *473*, 24 - 32. Retrieved from http://www.sciencedirect.com/science/article/pii/

S0012821X17303060 doi: https://doi.org/10.1016/j.epsl.2017.05.038

Santamaría-Gómez, A., & Mémin, A. (2015, 05). Geodetic secular velocity errors due to interannual surface loading deformation. *Geophysical Journal International*, *202*(2), 763-767. Retrieved from https://doi.org/10.1093/gji/ggv190 doi: 10.1093/gji/ggv190

Sato, T., Okuno, J., Hinderer, J., MacMillan, D. S., Plag, H.-P., Francis, O., … Fukuda, Y. (2006, 06). A geophysical interpretation of the secular displacement and gravity rates observed at Ny-Ålesund, Svalbard in the Arctic—effects of post-glacial rebound and present-day ice melting. *Geophysical Journal International*, *165*(3), 729-743. Retrieved from https://doi.org/10.1111/j.1365-246X.2006.02992.x doi: 10.1111/j.1365-246X.2006.02992.x

Schröder, L., Horwath, M., Dietrich, R., Helm, V., van den Broeke, M. R., & Ligtenberg, S. R. M. (2019). Four decades of antarctic surface elevation changes from multi-mission satellite altimetry. *The Cryosphere*, *13*(2), 427–449. Retrieved from https://www.the-cryosphere.net/13/427/2019/ doi: 10.5194/tc-13-427-2019

Schumacher, M., King, M., Rougier, J., Sha, Z., Khan, S. A., & Bamber, J. (2018). A new global gps data set for testing and improving modelled gia uplift rates. *Geophysical Journal International*, *214*(3), 2164-2176. Retrieved from https://www.scopus.com/inward/record.uri?eid=2-s2.0-85050475763&doi=10.1093%2fgji%2fggy235&partnerID=40&md5=0b6d3ed0cdf0208346d1d8bb4bed2c40 (cited By 5) doi: 10.1093/gji/ggy235

Simon, K. M., Riva, R. E. M., Kleinherenbrink, M., & Frederikse, T. (2018). The glacial isostatic adjustment signal at present day in northern europe and the british isles estimated from geodetic observations and geophysical models. *Solid Earth*, *9*(3), 777–795. Retrieved from https://www.solid-earth.net/9/777/2018/ doi: 10.5194/se-9-777-2018

Smith, B. E., Fricker, H. A., Joughin, I. R., & Tulaczyk, S. (2009). An inventory of active subglacial lakes in antarctica detected by icesat (2003–2008). *Journal of Glaciology*, *55*(192), 573–595. doi: 10.3189/002214309789470879

Sun, Y., Riva, R., & Ditmar, P. (2016). Optimizing estimates of annual variations and trends in geocenter motion and j2 from a combination of grace data and geophysical models. *Journal of Geophysical Research: Solid Earth*, *121*(11), 8352-8370. Retrieved from https://agupubs.onlinelibrary.wiley.com/doi/abs/10.1002/2016JB013073 doi: 10.1002/2016JB013073

Sørensen, L. S., Jarosch, A. H., Adalgeirsdóttir, G., Barletta, V. R., Forsberg, R., Pálsson, F., … Jóhannesson, T. (2017, 01). The effect of signal leakage and glacial isostatic rebound on GRACE-derived ice mass changes in Iceland. *Geophysical Journal International*, *209*(1), 226-233. Retrieved from https://doi.org/10.1093/gji/ggx008 doi: 10.1093/gji/ggx008

Tapley, B. D., Bettadpur, S., Watkins, M., & Reigber, C. (2004). The gravity recovery and climate experiment: Mission overview and early results. *Geophysical Research Letters*, *31*(9). Retrieved from https://agupubs.onlinelibrary.wiley.com/doi/abs/10.1029/2004GL019920 doi: 10.1029/2004GL019920

Tushingham, A. M., & Peltier, W. R. (1991). Ice-3g: A new global model of late pleistocene deglaciation based upon geophysical predictions of post-glacial relative sea level change. *Journal of Geophysical Research: Solid Earth*, *96*(B3), 4497-4523. Retrieved from https://agupubs.onlinelibrary.wiley.com/doi/abs/10.1029/90JB01583 doi: 10.1029/90JB01583

van Dam, T., Collilieux, X., Wuite, J., Altamimi, Z., & Ray, J. (2012). Nontidal ocean loading: amplitudes and potential effects in gps height time series. *Journal of Geodesy*, *86*(11), 1043–1057. Retrieved from https://doi.org/10.1007/s00190-012-0564-5 doi: 10.1007/s00190-012-0564-5

VanLooy, J., Forster, R., & Ford, A. (2006). Accelerating thinning of kenai peninsula glaciers, alaska. *Geophysical Research Letters*, *33*(21). Retrieved from https://agupubs.onlinelibrary.wiley.com/doi/abs/10.1029/2006GL028060 doi: 10.1029/2006GL028060

Wang, H., Xiang, L., Jia, L., Jiang, L., Wang, Z., Hu, B., & Gao, P. (2012). Load love numbers and green's functions for elastic earth models prem, iasp91, ak135, and modified models with refined crustal structure from crust 2.0. *Computers & Geosciences*, *49*, 190 - 199. Retrieved from http://www.sciencedirect.com/science/article/pii/S0098300412002245 doi: https://doi.org/10.1016/j.cageo.2012.06.022

Watson, C. S., White, N. J., Church, J. A., King, M. A., Burgette, R. J., & Legresy, B. (2015, JUN). Unabated global mean sea-level rise over the satellite altimeter era. *NATURE CLIMATE CHANGE*, *5*(6), 565+.

Whitehouse, P. L., Allen, M. B., & Milne, G. A. (2007, 08). Glacial isostatic adjustment as a control on coastal processes: An example from the Siberian Arctic. *Geology*, *35*(8), 747-750. Retrieved from https://doi.org/10.1130/G23437A.1 doi: 10.1130/G23437A.1

Wöppelmann, G., & Marcos, M. (2016). Vertical land motion as a key to understanding sea level change and variability. *Reviews of Geophysics*, *54*(1), 64-92. Retrieved from https://agupubs.onlinelibrary.wiley.com/doi/abs/10.1002/2015RG000502 doi: 10.1002/2015RG000502

Zemp, M., Huss, M., Thibert, E., Eckert, N., McNabb, R., Huber, J., … Cogley, J. G. (2019). Global glacier mass changes and their contributions to sea-level rise from 1961 to 2016. *Nature*, *568*(7752), 382-386. doi: 10.1038/s41586-019-1071-0

Zwally, H. J., Schutz, R., Bentley, C., Bufton, J., Herring, T., Minster, J., … Thomas, R. (2011). *Glas/icesat l2 antarctic and greenland ice sheet altimetry data v031.* (Boulder, Colorado: NASA Distributed Active Archive Center at the National Snow and Ice Data Center) doi: 10.5067/CPRXXK3F39RV

References of Supporting Information:

Caron, L., Ivins, E. R., Larour, E., Adhikari, S., Nilsson, J., & Blewitt, G. (2018). Gia model statistics for grace hydrology, cryosphere, and ocean science. *Geophysical Research Letters*, *45*(5), 2203-2212. Retrieved from https://agupubs.onlinelibrary.wiley.com/doi/abs/10.1002/2017GL076644 doi: 10.1002/2017GL076644

Cohen, S. C., & Freymueller, J. T. (2001). Crustal uplift in the south central alaska subduction zone: New analysis and interpretation of tide gauge observations. *Journal of Geophysical Research: Solid Earth*, *106*(B6), 11259-11270. Retrieved from https://agupubs.onlinelibrary.wiley.com/doi/abs/10.1029/2000JB900419 doi: 10.1029/2000JB900419

Fleming, K., Martinec, Z., & Wolf, D. (2007, 01). Glacial-isostatic adjustment and the viscosity structure underlying the vatnajökull ice cap, iceland. *Pure and Applied Geophysics*, *164*, 751-768. doi: 10.1007/s00024-007-0187-6

Frederikse, T., Landerer, F. W., & Caron, L. (2019). The imprints of contemporary mass redistribution on local sea level and vertical land motion observations. *Solid Earth*, *10*(6), 1971–1987. Retrieved from https://www.solid-earth.net/10/1971/2019/ doi: 10.5194/se-10-1971-2019

Grove, J. (2001, 01). The initiation of the "little ice age" in regions round the north atlantic. *Climatic Change*, *48*, 53-82. doi: 10.1023/A:1005662822136

Hu, Y., & Freymueller, J. T. (2019). Geodetic observations of time-variable glacial isostatic adjustment in southeast alaska and its implications for earth rheology. *Journal of Geophysical Research: Solid Earth*, *124*(9), 9870-9889. Retrieved from https://agupubs.onlinelibrary.wiley.com/doi/abs/10.1029/2018JB017028 doi: 10.1029/2018JB017028

Kierulf, H. P., Plag, H.-P., & Kohler, J. (2009, 10). Surface deformation induced by present-day ice melting in Svalbard. *Geophysical Journal International*, *179*(1), 1-13. Retrieved from https://doi.org/10.1111/j.1365-246X.2009.04322.x doi: 10.1111/j.1365-246X.2009.04322.x

King, M. A., & Watson, C. S. (2014, 09). Geodetic vertical velocities affected by recent rapid changes in polar motion. *Geophysical Journal International*, *199*(2), 1161-1165. Retrieved from https://doi.org/10.1093/gji/ggu325 doi: 10.1093/gji/ggu325

Larsen, C. F., Motyka, R. J., Freymueller, J. T., Echelmeyer, K. A., & Ivins, E. R. (2005). Rapid viscoelastic uplift in southeast alaska caused by post-little ice age glacial retreat. *Earth and Planetary Science Letters*, *237*(3), 548 - 560. Retrieved from http://www.sciencedirect.com/science/article/pii/S0012821X05004152 doi: https://doi.org/10.1016/j.epsl.2005.06.032

Mémin, A., Spada, G., Boy, J.-P., Rogister, Y., & Hinderer, J. (2014, 05). Decadal geodetic variations in Ny-Ålesund (Svalbard): role of past and present ice-mass changes . *Geophysical Journal International*, *198*(1), 285-297. Retrieved from https://doi.org/10.1093/gji/ggu134 doi: 10.1093/gji/ggu134

Peltier, W., Argus, D., & Drummond, R. (2015). Space geodesy constrains ice age terminal deglaciation: The global ice-6g-c (vm5a) model. *Journal of Geophysical Research: Solid Earth*, *120*(1), 450-487. Retrieved from https://www.scopus.com/inward/record.uri?eid=2-s2.0-85027948080&doi=10.1002%2f2014JB011176&partnerID=40&md5=29a7ce38c5cf3872d2276981d2f6b34f (cited By 326) doi: 10.1002/2014JB011176

Pfeffer, W. T., Arendt, A. A., Bliss, A., Bolch, T., Cogley, J. G., Gardner, A. S., … et al. (2014). The randolph glacier inventory: a globally complete inventory of glaciers. *Journal of Glaciology*, *60*(221), 537–552. doi: 10.3189/2014JoG13J176

Rajner, M. (2018). Detection of ice mass variation using gnss measurements at svalbard. *Journal of Geodynamics*, *121*, 20 - 25. Retrieved from http://www.sciencedirect.com/science/article/pii/S0264370718300450 doi: https://doi.org/10.1016/j.jog.2018.06.001

Root, B. C., Tarasov, L., & van der Wal, W. (2015). Grace gravity observations constrain weichselian ice thickness in the barents sea. *Geophysical Research Letters*, *42*(9), 3313-3320. Retrieved from https://agupubs.onlinelibrary.wiley.com/doi/abs/10.1002/2015GL063769 doi: 10.1002/2015GL063769

Sato, T., Okuno, J., Hinderer, J., MacMillan, D. S., Plag, H.-P., Francis, O., … Fukuda, Y. (2006, 06). A geophysical interpretation of the secular displacement and gravity rates observed at Ny-Ålesund, Svalbard in the Arctic—effects of post-glacial rebound and present-day ice melting. *Geophysical Journal International*, *165*(3), 729-743. Retrieved from https://doi.org/10.1111/j.1365-246X.2006.02992.x doi: 10.1111/j.1365-246X.2006.02992.x

Schröder, L., Horwath, M., Dietrich, R., Helm, V., van den Broeke, M. R., & Ligtenberg, S. R. M. (2019). Four decades of antarctic surface elevation changes from multi-mission satellite altimetry. *The Cryosphere*, *13*(2), 427–449. Retrieved from https://www.the-cryosphere.net/13/427/2019/ doi: 10.5194/tc-13-427-2019

Shepherd, A., Ivins, E., Rignot, E., Smith, B., van den Broeke, M., Velicogna, I., … Wouters, B. (2018). Mass balance of the antarctic ice sheet from 1992 to 2017. *Nature*, *558*(7709), 219–222. doi: 10.1038/s41586-018-0179-y

Sun, Y., Riva, R., & Ditmar, P. (2016). Optimizing estimates of annual variations and trends in geocenter motion and j2 from a combination of grace data and geophysical models. *Journal of Geophysical Research: Solid Earth*, *121*(11), 8352-8370. Retrieved from https://agupubs.onlinelibrary.wiley.com/doi/abs/10.1002/2016JB013073 doi: 10.1002/2016JB013073

Swenson, S., Chambers, D., & Wahr, J. (2008). Estimating geocenter variations from a combination of grace and ocean model output. *Journal of*

Geophysical Research: Solid Earth, *113*(B8). Retrieved from https://agupubs.onlinelibrary.wiley.com/doi/abs/10.1029/2007JB005338 doi: 10.1029/2007JB005338

Sørensen, L. S., Jarosch, A. H., Adalgeirsdóttir, G., Barletta, V. R., Forsberg, R., Pálsson, F., … Jóhannesson, T. (2017, 01). The effect of signal leakage and glacial isostatic rebound on GRACE-derived ice mass changes in Iceland. *Geophysical Journal International*, *209*(1), 226-233. Retrieved from https://doi.org/10.1093/gji/ggx008 doi: 10.1093/gji/ggx008

Tushingham, A. M., & Peltier, W. R. (1991). Ice-3g: A new global model of late pleistocene deglaciation based upon geophysical predictions of post-glacial relative sea level change. *Journal of Geophysical Research: Solid Earth*, *96*(B3), 4497-4523. Retrieved from https://agupubs.onlinelibrary.wiley.com/doi/abs/10.1029/90JB01583 doi: 10.1029/90JB01583

VanLooy, J., Forster, R., & Ford, A. (2006). Accelerating thinning of kenai peninsula glaciers, alaska. *Geophysical Research Letters*, *33*(21). Retrieved from https://agupubs.onlinelibrary.wiley.com/doi/abs/10.1029/2006GL028060 doi: 10.1029/2006GL028060

Whitehouse, P. L., Allen, M. B., & Milne, G. A. (2007, 08). Glacial isostatic adjustment as a control on coastal processes: An example from the Siberian Arctic. *Geology*, *35*(8), 747-750. Retrieved from https://doi.org/10.1130/G23437A.1 doi: 10.1130/G23437A.1

Supporting Information for "Vertical Land Motion from Present-Day Deglaciation in the Wider Arctic"

Carsten Ankjær Ludwigsen[1], Shfaqat Abbas Khan[1], Ole Baltazar Andersen[1] and Ben Marzeion[2]

[1]DTU Space, Technical University of Denmark
[2]Institute of Geography and MARUM Center for Marine Environmental Sciences, University of Bremen, Germany

Contents of this file

S1 Description of glacier ice model

As initial conditions, we use glacier outlines obtained from RGI6.0 (Pfeffer et al., 2014). The time stamp of these outlines differs between glaciers, but is typically around the year 2000. To obtain results before this time, the model uses an iterative process to find the glacier geometry in the year of initialization (e.g., 1901) that results in the observed glacier geometry in the year of the outlines time stamp (e.g., 2000) after the model was run forward.

The model relies on monthly temperature and precipitation anomalies to calculate the specific mass balance of each glacier. Here, we use the mean of seven different reanalysis products as boundary conditions. Temperature is used to estimate the ablation of glaciers following a temperature-index melt model, and to estimate the solid fraction of total precipitation, which is used to estimate accumulation.

Mass balance data for each glacier is distributed over the glacier according to a mathematical approximation, assuming conservation of mass and that the glacier has a elevation gain at the top which becomes a elevation decline further down the glacier. The altitude where the elevation change goes from positive to negative, E, is approximated by a simple function of the glacial altitude (Z) and the averaged ice height change, ($\bar{\mathrm{h}} = \rho b A^{-1}$), and ρ is the ice density (917 kg m^{-3}). Note that E is different from the equilibrium line altitude (ELA).

$$\mathrm{E} = (1-\bar{\mathrm{h}})\tilde{Z} \tag{S1}$$

where $\tilde{Z}$ is the median glacial height. For every glacier we define a distribution function, $D(i)$, where i represents a grid cell of the glacier:

$$D(i) = \quad 1 - \exp\left(\frac{(2-\bar{\mathrm{h}})(\mathrm{E}-Z(i))}{Z_{max}}\right) \tag{S2}$$

For all glaciers, is the elevation change assumed to be exponentially declining with height, $Z(i)$. The fraction in the exponential term makes sure that glaciers that on average gains

Corresponding author: Carsten Ankjær Ludwigsen, caanlu@space.dtu.dk

up to 2 m height, will have an elevation loss in the bottom of the glacier and elevation gain at the top, unless E is equal or to Z_{max}, in which case, the whole glacier will be loosing height.

The elevation change, dh/dt, is found by normalizing D, multiplying with the total mass balance, b, and converted to a height change by dividing with $\rho = 917$ kg m^{-3}.

$$\frac{dh(i)}{dt} = \frac{b}{\rho}\hat{D}(i) \qquad \text{where,} \tag{S3}$$

$$\hat{D}(i) = \frac{D(i)}{\sum_{i=1}^{k} D(i)} \tag{S4}$$

S1.1 Data availability

The ice model is available as a NetCDF-4 file on `data.dtu.dk/articles/Arctic_Vertical_Land_Motion_5x5_km_/12554489`.

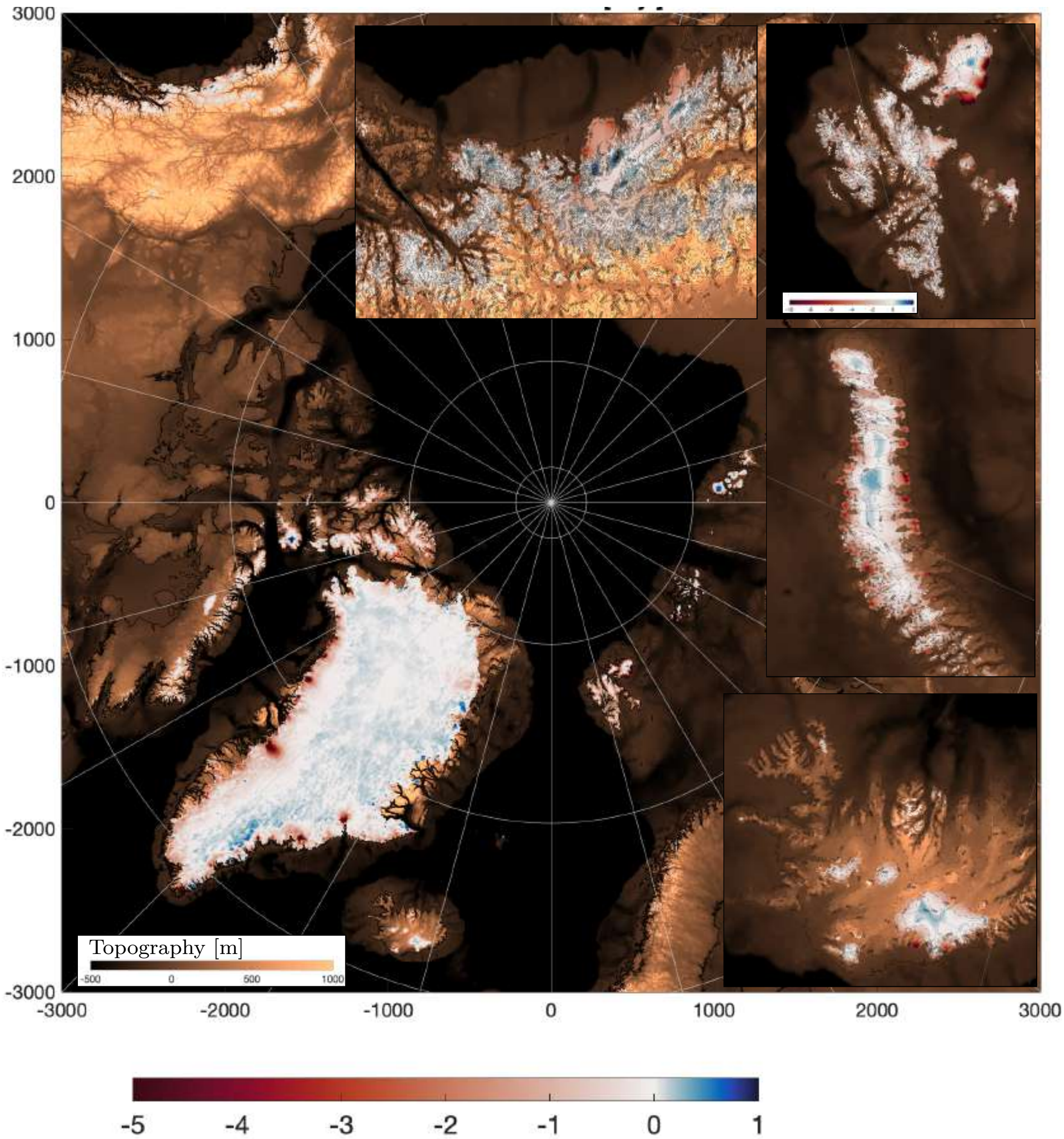

Figure S1.1. Ice elevation change from 2003 to 2015 in m yr^{-1} (red-blue scale) resulting from the redistribution explained above. The most interesting regions (Alaskian Coast, Svalbard (on a wider colorscale), Novaya Zemlja and Iceland) are enlarged. There is no significant ice loss in mainland Siberia. The elevation change is not comparable with actual elevation change, since no model for firn has been applied. The values on the map a proportional with mass changes (assumed density of 917 kg m^{-3})

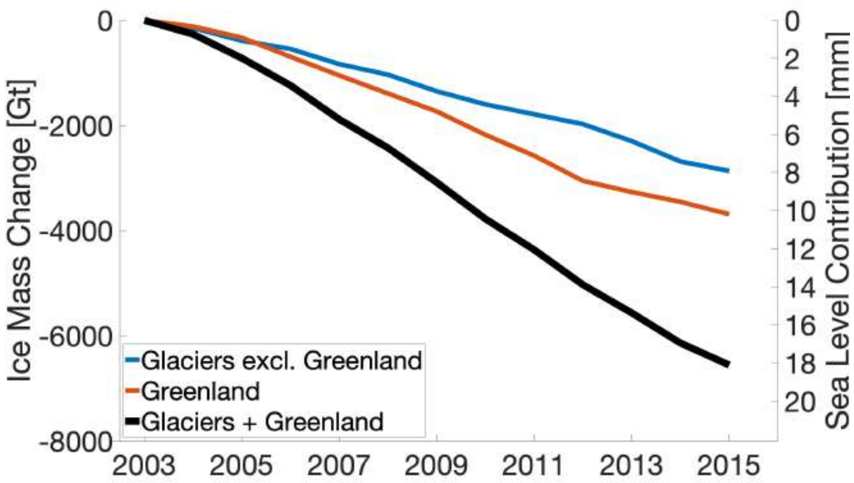

Figure S1.2. Ice loss from Greenland (including peripheral glaciers) and Arctic glaciers that goes in to the VLM calculations.

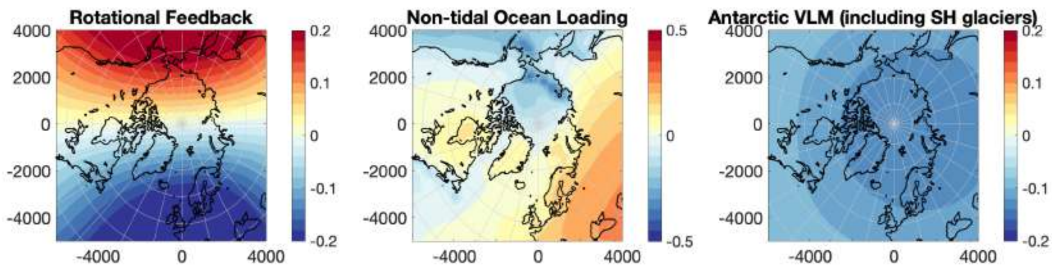

Figure S2.1. 2003-2015 average trends of rotational feedback, Non-tidal ocean loading and Antarctic elastic VLM fingerprint [mm yr^{-1}].

S2 Influence of rotational feedback, ocean loading and Antarctic ice loss

Rotational feedback is calculated using the eq.1 and eq.2 by King and Watson (2014). Pole positions x_p, y_p used in the calculations are available from `https://datacenter.iers.org/eop.php`. The Geocenter Motion subtracted from GNSS calculated as described in (Swenson et al., 2008) uses the degree-1 stokes coefficients based on the calculations by Sun et al. (2016) are available from `https://grace.jpl.nasa.gov/data/get-data/geocenter/`. The associated uncertainity of the geocenter motion has been added to the GNSS-error estimate. The elastic VLM effect of Antarctic Ice Loss is estimated from elevation changes by Schröder et al. (2019), which had an average mass loss of 105 Gt yr^{-1} between 2003 and 2015 which agrees well with the result of IMBIE(Shepherd et al., 2018).

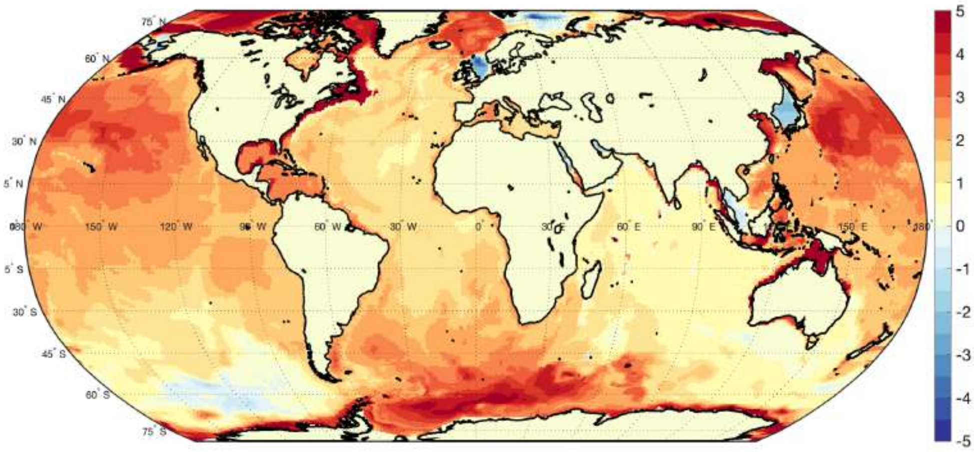

Figure S2.2. 2003-2015 ocean mass trend [mm/y] from ECCOv4r4 OBP used to estimate the effect of NOL.

S3 Spatial distributions of of the VLM-model error

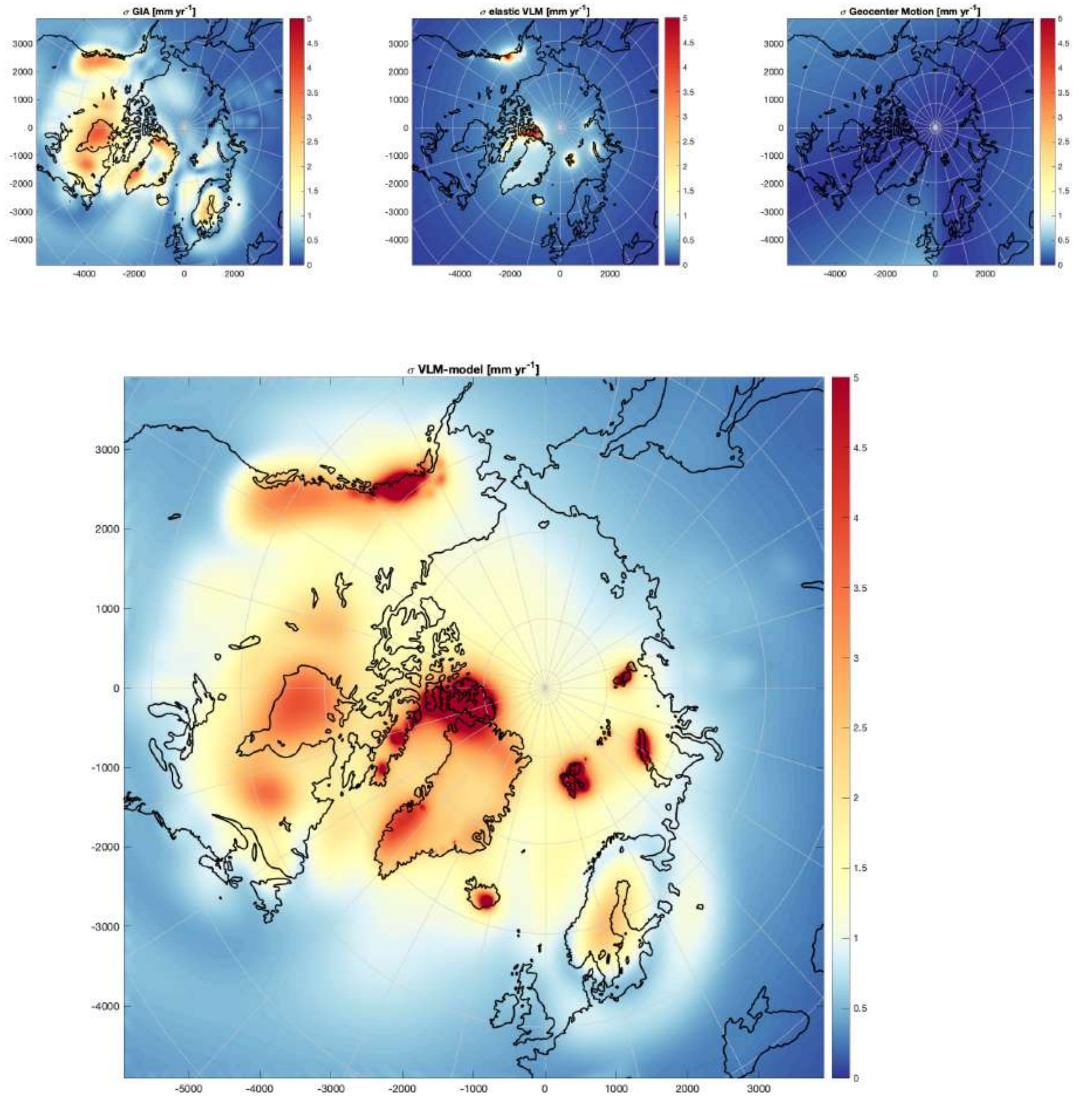

Figure S3.1. Standard deviation (σ) of GIA, elastic VLM and Geocenter Motion and combined for the total VLM-model [mm/yr] for 2003-2015.

S4 VLM at GNSS-sites

In this section, we explain the VLM measured by GNSS in comparison to the VLM-model for the regions covered in this study.

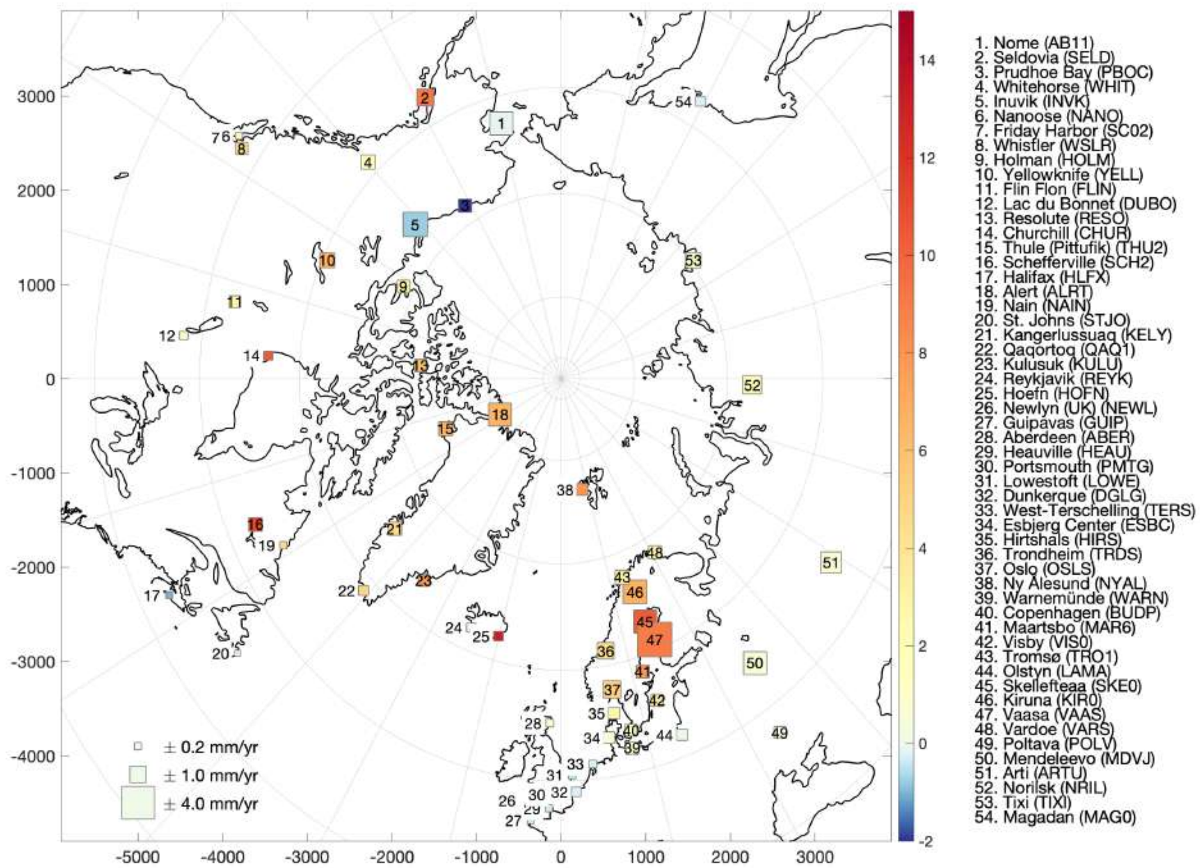

Figure S4.1. Location and name (and IGS abbreviation) of the 42 GNSS-sites used in this study ordered from most west to most east. The color indicates the linear trend from 2003-2015 [mm yr^{-1}], while the size of the square is proportional with the standard error (as estimated in the URL6-product).

S5 Timeseries of vertical deformation at all GNSS sites

Figure S5.1 shows both measured and modeled vertical deformation from 2003-2015 of each individual GNSS-site. It also reflects, how elastic VLM is changing year by year, while GIA is linear.

S6 Contribution of elastic VLM and GIA

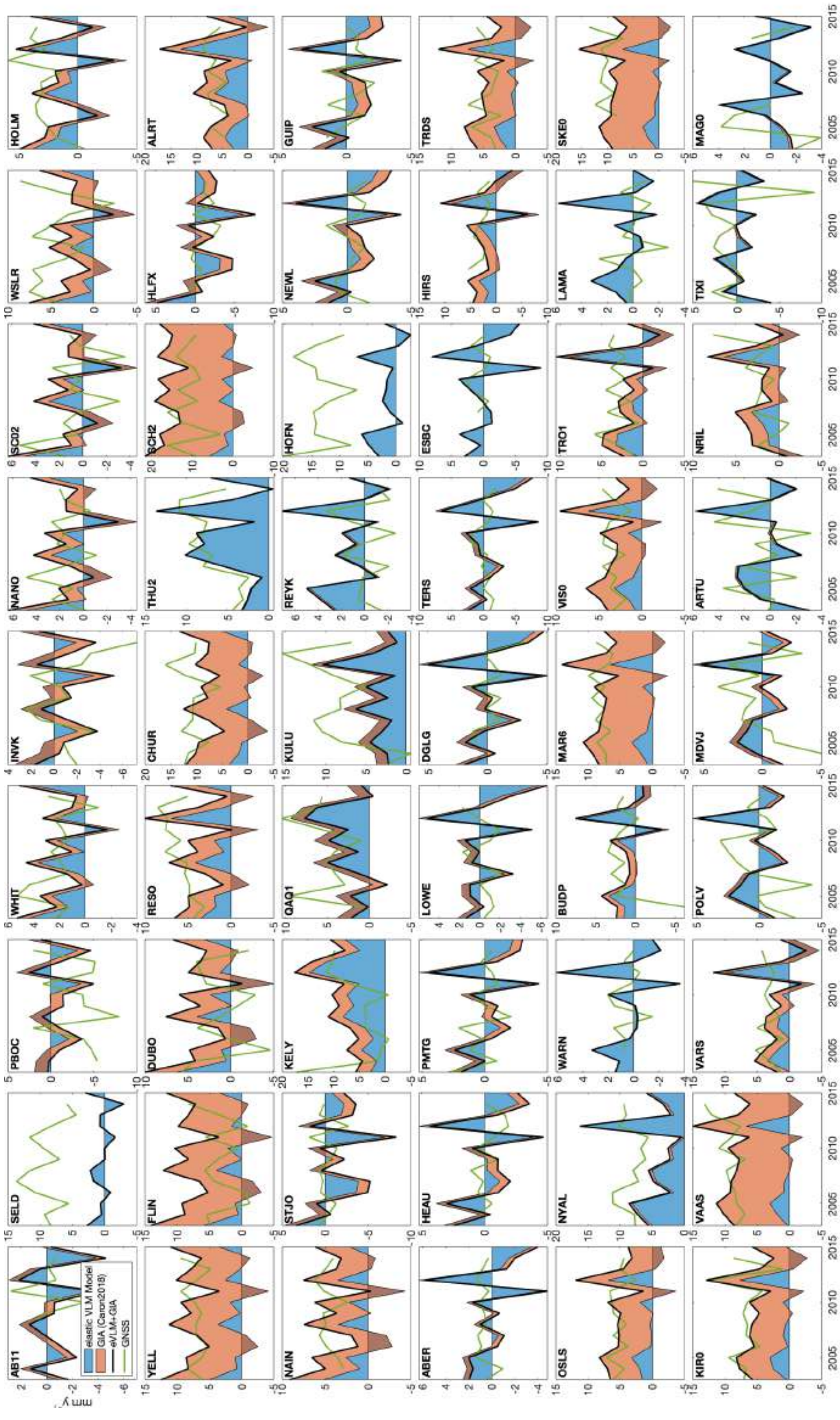

Figure S5.1. Measured and predicted year-to-year VLM-change [mm y^{-1}] from 2003 to 2015 for the 54 GNSS locations. GNSS is shown by the green line and the VLM model by the black line. The red and blue areas indicate the part of the VLM model that is elastic and GIA.

	IGS id	Abbr.	elastic VLM	Caron2018	VLM-model	GNSS VLM	Residual
Nome	4	AB11	-0.4 ± 0.7	-0.8 ± 0.3	-1.1 ± 1.0	-0.1 ± 0.9	-1.0 ± 1.4
Seldovia	517	SELD	0.3 ± 1.6	-0.1 ± 0.8	0.2 ± 2.4	9.2 ± 1.0	-9.0 ± 2.6
Prudhoe Bay	433	PBOC	0.1 ± 0.9	-1.5 ± 0.5	-1.4 ± 1.4	-3.2 ± 1.6	1.8 ± 2.1
Whitehorse	651	WHIT	1.1 ± 2.6	0.9 ± 1.3	2.0 ± 3.9	2.0 ± 0.8	0.0 ± 4.0
Inuvik	232	INVK	0.3 ± 1.0	-1.7 ± 0.9	-1.4 ± 1.9	-0.8 ± 1.0	-0.6 ± 2.1
Nanoose	341	NANO	-0.1 ± 0.6	1.5 ± 2.7	1.5 ± 3.3	1.6 ± 1.0	-0.2 ± 3.4
Friday Harbor	508	SC02	-0.2 ± 0.5	1.3 ± 2.6	1.1 ± 3.1	0.4 ± 1.3	0.7 ± 3.4
Whistler	656	WSLR	0.3 ± 0.6	2.5 ± 3.1	2.8 ± 3.8	4.5 ± 1.3	-1.7 ± 4.0
Holman	218	HOLM	0.3 ± 1.0	1.1 ± 0.8	1.4 ± 1.8	3.1 ± 1.1	-1.7 ± 2.1
Yellowknife	664	YELL	0.4 ± 0.8	7.6 ± 1.5	8.0 ± 2.3	6.8 ± 0.8	1.2 ± 2.4
Flin Flon	168	FLIN	0.2 ± 0.6	8.3 ± 1.6	8.4 ± 2.2	3.0 ± 0.9	5.4 ± 2.4
Lac du Bonnet	143	DUBO	0.1 ± 0.5	3.7 ± 1.1	3.8 ± 1.6	1.0 ± 0.9	2.8 ± 1.8
Resolute	477	RESO	1.1 ± 2.2	3.1 ± 0.9	4.2 ± 3.1	6.0 ± 1.2	-1.8 ± 3.3
Churchill	106	CHUR	0.4 ± 0.7	8.4 ± 2.8	8.8 ± 3.5	10.4 ± 0.8	-1.6 ± 3.6
Thule (Pittufik)	583	THU2	5.3 ± 3.3	0.1 ± 2.1	5.4 ± 5.4	6.6 ± 0.9	-1.2 ± 5.5
Schefferville	510	SCH2	0.4 ± 0.6	15.7 ± 2.3	16.1 ± 2.9	11.0 ± 0.7	5.0 ± 3.0
Halifax	211	HLFX	-0.5 ± 0.4	-1.5 ± 0.8	-2.0 ± 1.2	-1.1 ± 1.6	-0.9 ± 2.0
Alert	27	ALRT	3.4 ± 4.0	4.1 ± 1.5	7.6 ± 5.6	6.6 ± 1.2	1.0 ± 5.7
Nain	340	NAIN	0.4 ± 0.7	4.0 ± 1.0	4.4 ± 1.7	4.6 ± 1.5	-0.2 ± 2.3
St. Johns	548	STJO	-0.5 ± 0.4	-1.4 ± 0.3	-1.8 ± 0.8	-0.2 ± 0.8	-1.6 ± 1.1
Kangerlussuaq	247	KELY	6.6 ± 2.5	2.9 ± 3.4	9.4 ± 5.8	4.6 ± 1.2	4.8 ± 5.9
Qaqortoq	467	QAQ1	4.1 ± 1.5	-1.7 ± 1.4	2.4 ± 2.8	4.9 ± 0.8	-2.5 ± 3.0
Kulusuk	265	KULU	5.1 ± 1.6	-1.5 ± 1.0	3.6 ± 2.6	7.8 ± 1.0	-4.2 ± 2.8
Reykjavik	479	REYK	1.4 ± 1.4	0.2 ± 1.4	1.6 ± 2.8	-0.0 ± 1.1	1.6 ± 3.1
Hoefn	215	HOFN	1.9 ± 3.9	-0.1 ± 1.0	1.8 ± 4.9	13.1 ± 1.1	-11.3 ± 5.1
Newlyn (UK)	347	NEWL	0.1 ± 0.4	-1.1 ± 0.2	-0.9 ± 0.6	-0.2 ± 1.3	-0.7 ± 1.4
Guipavas	202	GUIP	0.2 ± 0.3	-1.0 ± 0.2	-0.9 ± 0.6	-0.4 ± 1.7	-0.4 ± 1.8
Aberdeen	10	ABER	0.4 ± 0.5	-0.5 ± 0.4	-0.1 ± 0.9	0.9 ± 1.2	-1.0 ± 1.5
Heauville	206	HEAU	0.1 ± 0.3	-0.8 ± 0.2	-0.7 ± 0.6	-0.3 ± 1.5	-0.4 ± 1.6
Portsmouth	446	PMTG	0.3 ± 0.4	-0.8 ± 0.3	-0.5 ± 0.6	0.1 ± 1.2	-0.6 ± 1.4
Lowestoft	286	LOWE	0.1 ± 0.4	-0.8 ± 0.5	-0.7 ± 0.9	-0.4 ± 1.8	-0.2 ± 2.0
Dunkerque	134	DGLG	0.2 ± 0.4	-0.7 ± 0.5	-0.6 ± 0.8	-0.3 ± 0.9	-0.3 ± 1.2
West-Terschelling	568	TERS	0.1 ± 0.4	-0.9 ± 0.7	-0.8 ± 1.1	-0.2 ± 0.8	-0.6 ± 1.4
Esbjerg Center	153	ESBC	0.3 ± 0.4	-0.1 ± 0.5	0.2 ± 0.9	0.6 ± 0.8	-0.4 ± 1.2
Hirtshals	210	HIRS	0.4 ± 0.5	2.2 ± 0.8	2.7 ± 1.3	2.8 ± 1.9	-0.1 ± 2.3
Trondheim	596	TRDS	0.8 ± 0.6	4.6 ± 1.1	5.4 ± 1.7	4.3 ± 0.8	1.1 ± 1.9
Oslo	378	OSLS	0.7 ± 0.5	5.0 ± 1.8	5.7 ± 2.3	5.2 ± 0.8	0.5 ± 2.4
Ny Ålesund	370	NYAL	4.6 ± 5.3	0.5 ± 0.4	5.1 ± 5.7	7.9 ± 0.9	-2.9 ± 5.7
Warnemünde	647	WARN	0.6 ± 0.4	-0.1 ± 0.5	0.5 ± 0.9	0.6 ± 0.8	-0.0 ± 1.2
Copenhagen	75	BUDP	0.6 ± 0.4	0.9 ± 0.5	1.6 ± 0.9	1.6 ± 3.7	-0.1 ± 3.8
Maartsbo	306	MAR6	0.8 ± 0.5	7.6 ± 2.4	8.3 ± 2.9	7.8 ± 0.8	0.5 ± 3.0
Visby	639	VIS0	0.8 ± 0.4	3.3 ± 1.1	4.0 ± 1.6	3.3 ± 0.8	0.8 ± 1.8
Tromsø	599	TRO1	0.9 ± 0.8	1.7 ± 0.7	2.5 ± 1.5	3.0 ± 0.8	-0.5 ± 1.7
Olstyn	274	LAMA	0.7 ± 0.4	0.1 ± 0.5	0.8 ± 0.9	-0.0 ± 0.7	0.8 ± 1.2
Skellefteaa	534	SKE0	0.9 ± 0.6	8.5 ± 2.1	9.4 ± 2.7	10.3 ± 7.0	-0.9 ± 7.5
Kiruna	252	KIR0	0.9 ± 0.7	5.2 ± 0.9	6.1 ± 1.6	6.8 ± 0.8	-0.6 ± 1.8
Vaasa	625	VAAS	0.9 ± 0.6	8.3 ± 2.2	9.1 ± 2.7	9.0 ± 0.9	0.1 ± 2.9
Vardoe	630	VARS	0.9 ± 0.8	2.0 ± 0.6	2.9 ± 1.4	3.0 ± 0.9	-0.2 ± 1.7
Poltava	452	POLV	0.7 ± 0.3	-0.4 ± 0.3	0.2 ± 0.5	0.2 ± 1.0	0.0 ± 1.1
Mendeleevo	323	MDVJ	0.8 ± 0.4	-0.7 ± 0.8	0.2 ± 1.2	0.7 ± 1.1	-0.5 ± 1.6
Arti	36	ARTU	0.8 ± 0.3	-0.2 ± 0.2	0.6 ± 0.6	0.7 ± 0.9	-0.1 ± 1.0
Norilsk	360	NRIL	0.9 ± 0.6	1.9 ± 0.2	2.8 ± 0.8	1.8 ± 0.8	1.0 ± 1.2
Tixi	587	TIXI	0.2 ± 0.6	-0.3 ± 0.3	-0.1 ± 0.9	1.0 ± 1.0	-1.1 ± 1.3
Magadan	298	MAG0	-0.2 ± 0.3	-0.2 ± 0.2	-0.4 ± 0.5	-0.3 ± 1.0	-0.1 ± 1.2

Table S4.1. Measured and modelled VLM for each GNSS-site in mm yr^{-1}. VLM-model is the sum of elastic VLM and GIA VLM.

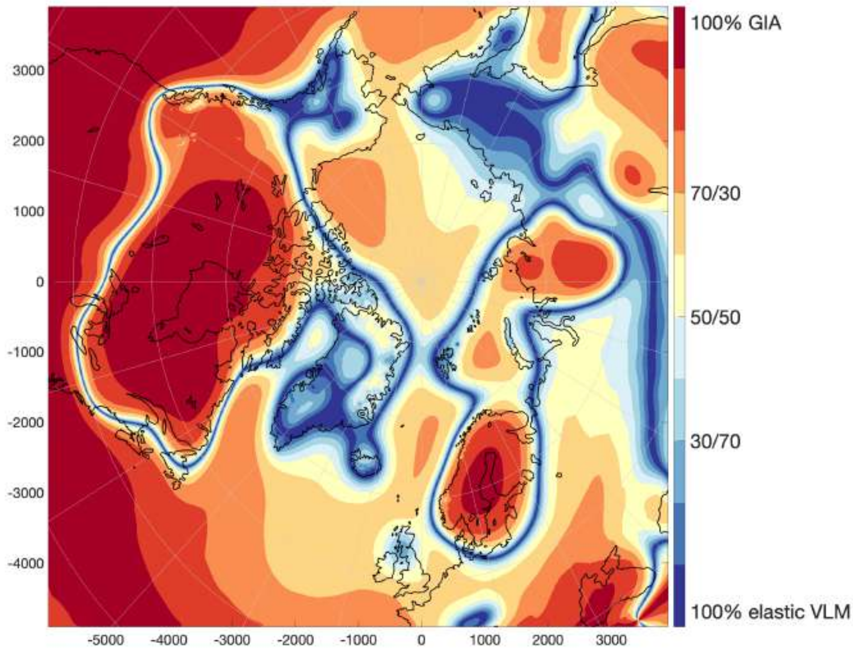

Figure S6.1. Percentage contribution of GIA-rate and elastic VLM-rate to total VLM-rate (in absolute terms) are shown. Red colors indicate areas in which GIA dominates VLM, while blue colors indicate areas in which elastic VLM is dominant.

References

King, M. A., & Watson, C. S. (2014, 09). Geodetic vertical velocities affected by recent rapid changes in polar motion. *Geophysical Journal International*, *199*(2), 1161-1165. Retrieved from `https://doi.org/10.1093/gji/ggu325` doi: 10.1093/gji/ggu325

Pfeffer, W. T., Arendt, A. A., Bliss, A., Bolch, T., Cogley, J. G., Gardner, A. S., . . . et al. (2014). The randolph glacier inventory: a globally complete inventory of glaciers. *Journal of Glaciology*, *60*(221), 537552. doi: 10.3189/2014JoG13J176

Schröder, L., Horwath, M., Dietrich, R., Helm, V., van den Broeke, M. R., & Ligtenberg, S. R. M. (2019). Four decades of antarctic surface elevation changes from multi-mission satellite altimetry. *The Cryosphere*, *13*(2), 427–449. Retrieved from `https://www.the-cryosphere.net/13/427/2019/` doi: 10.5194/tc-13-427-2019

Shepherd, A., Ivins, E., Rignot, E., Smith, B., van den Broeke, M., Velicogna, I., . . . Wouters, B. (2018). Mass balance of the antarctic ice sheet from 1992 to 2017. *Nature*, *558*(7709), 219–222. doi: 10.1038/s41586-018-0179-y

Sun, Y., Riva, R., & Ditmar, P. (2016). Optimizing estimates of annual variations and trends in geocenter motion and j2 from a combination of grace data and geophysical models. *Journal of Geophysical Research: Solid Earth*, *121*(11), 8352-8370. Retrieved from `https://agupubs.onlinelibrary.wiley.com/doi/abs/10.1002/2016JB013073` doi: 10.1002/2016JB013073

Swenson, S., Chambers, D., & Wahr, J. (2008). Estimating geocenter variations from a combination of grace and ocean model output. *Journal of Geophysical Research: Solid Earth*, *113*(B8). Retrieved from `https://agupubs.onlinelibrary.wiley.com/doi/abs/10.1029/2007JB005338` doi: 10.1029/2007JB005338